MISSISSIPPI RIVER PLUME VARIABILITY IN THE GULF OF MEXICO DERIVED FROM SMAP AND MODIS-AQUA

by

CAROLINA ERNANI DA SILVA

(Under the Direction of Renato M. Castelao)

ABSTRACT

The Mississippi River is an important source of freshwater and of terrigenous material to the Gulf of Mexico (GoM). This study aims to describe the Mississippi River Plume (MRP) seasonality and its interaction with the GoM circulation. We used terrigenous dissolved organic carbon from MODIS-Aqua and sea surface salinity from Soil Moisture Active Passive (SMAP) satellite to trace the distribution of the river plume in the coastal ocean. For the first time, the frequency of plume occurrence in the Gulf of Mexico was quantified. The MRP distribution on monthly time scales is controlled primarily by river discharge and by alongshore winds, with the maximum plume extension occurring during summer due to frequent reversions in winds. Two anomalous events in 2015 and 2016 demonstrated the importance of the interplay between upwelling-favorable winds, peaks in river discharge, the Loop Current and associated eddies on the offshore transport of MRP waters.

INDEX WORDS: Mississippi River, river plume, SMAP, tDOC, winds

MISSISSIPPI RIVER PLUME VARIABILITY IN THE GULF OF MEXICO DERIVED FROM SMAP AND MODIS-AQUA

by

CAROLINA ERNANI DA SILVA

BS, University of São Paulo 2015

A Thesis Submitted to the Graduate Faculty of The University of Georgia in Partial Fulfillment of the Requirements for the Degree

MASTER OF SCIENCE

ATHENS, GEORGIA

2018

MISSISSIPPI RIVER PLUME VARIABILITY IN THE GULF OF MEXICO DERIVED FROM SMAP AND MODIS-AQUA

by

CAROLINA ERNANI DA SILVA

BS, University of São Paulo 2015

Major Professor:	Renato M. Castelao
Committee:	C. Brock Woodson
	Daniela Di Iorio
	Patricia M. Medeiros
	Piero L. F. Mazzini

Electronic Version Approved:

Suzanne Barbour
Dean of the Graduate School
The University of Georgia
August 2018

ACKNOWLEDGEMENTS

This thesis will not be possible without the support of friends, family and my advisor. I would like to express my sincere gratitude to my advisor Renato M. Castelao for the continuous support, sharing his knowledge in innumerous discussions, patience, guidance through the master's degree process, and to make my journey in this country more friendly and smooth (e.g. with some cheese bread or Brazilian coffee).

I also would like to thank the committee members, Brock Woodson, Daniela Di Iorio, Patricia M Medeiros and Piero L. F. Mazzini, for their important feedbacks in this study.

Foremost, I would like to thank my family, Rosana (mother), Luiz (father), Gyovana (sister) and Fabricio (brother) that always taught me that nothing is impossible when you do that with love and hard work. Also, I am more than thankful for believe in me and their immense support, and kindness during my whole life. For you all my love.

My beloved partner, Matheus Maia Pacheco, which always was there for me, no matter the circumstances. You are the person that showed me that we can be stronger even when everything seems lost. I also would like to thank you to be my safe harbor, my best friend, my mentor, and my partner for this whole life. Everything that I do is thinking in us.

I also want to express my gratitude to my friends, Thassya and Igo, that make my graduation life healthier, spending some hours of their weekend with me on Skype no matter the distance and the time zone. To EJ who always, in a certain way, took care of

me, made the long distances of the cities in USA shorter with her kind and fun rides to the airport, grocery and restaurants and kept me positive during the master's degree. My lab mates Caitlin for always make my day sweeter with delicious homemade cupcakes, cakes and cute messages before I travel and Hilde for some delicious ice-cream in the end of the day, and great talks. Thank you all for being with me during these 2 years.

TABLE OF CONTENTS

LIST OF TABLES

Page

LIST OF FIGURES

Page

CHAPTER 1

INTRODUCTION

Rivers play a critical role on coastal circulation. They are the primary means by which freshwater, particles and dissolved materials are transported from land to the ocean. They have a great influence in the regional water cycle and biogeochemical processes. The Mississippi River (MR) is the largest river in North America with an average discharge of 13,500 ± 2,000 m^3 s^{-1} (Hu et al., 2005). It carries approximately 210 million tons of sediment into the Gulf of Mexico each year (Milliman and Meade, 1983). At the same time that these nutrient-rich waters are responsible for highly productive waters for fisheries (Chesney, Baltz and Thomas, 2000), they are also closely tied to the extensive development of summer-hypoxia in the Louisiana-Texas Shelf (LATEX, Rabalais et al., 1991; 2002).

Many processes can affect plume dispersal in the ocean, including wind forcing (Fong et al., 1997; Fong and Geyer, 2001; Choi and Wilkin, 2007), large-scale offshore currents (Huh et al., 1981) and eddies (Schiller et al., 2011). The MR discharges its water into the Gulf of Mexico, which is dominated by the Loop Current (LC) and by eddies that are frequently pinched off from the LC. Early investigations have suggested that the MR plume is mainly driven by winds near the coast (Cochrane and Kelly, 1986). Modeling studies (Schiller et al., 2011) have suggested that upwelling-favorable wind is the primary

mechanism for the offshore dispersal of the Mississippi River Plume (MRP). The Loop Current system and associated Loop Current Eddies (LCE) also have an important role in exporting low salinity water offshore (Huh et al., 1981; Schroeder et al., 1987; Hamilton and Lee, 2005; Schiller and Kourafalou, 2014), which in some cases can be transported beyond the Florida Strait (e.g., summer of 1993 – Walker et al., 1994; Gilbert et al., 1996; Del Castillo et al., 2001) into the Gulf Stream (e.g., summer of 2004 – Ortner et al., 1995; Hu et al., 2005). The relative contribution of these forcing mechanisms is currently not well understood.

Despite these advances, much remains to be learned about the distribution and variability of the Mississippi River plume in the northern Gulf of Mexico. Part of the challenge of studying the influence of river plumes in the coastal ocean is that, until recently, high quality satellite observations of sea surface salinity were not available. This restricted observational studies to depend either on short-term (e.g., a few weeks) shipboard surveys, or on point-measurements from moorings. The recent availability of satellite-derived observations of sea surface salinity, with the recent launch of Aquarius in 2011 and of the Soil Moisture Passive Active (SMAP) satellite in 2015, open a new window for characterizing river plume variability and its influence on coastal systems. As such, the main goal of this dissertation is to describe the seasonality of the Mississippi River plume in the Gulf of Mexico and to understand how physical forcing such as winds, river discharge, and large-scale circulation can influence its variability.

Chapter 2 addresses the description of the seasonality of the Mississippi River Plume based on terrigenous dissolved organic carbon (tDOC) derived from MODIS-Aqua and on sea surface salinity (SSS) derived from Soil Moisture Active Passive

(SMAP) measurements. An important goal of the analysis is to evaluate the effectiveness of the different satellite products as a tool to trace the river plume in the coastal ocean.

Lastly, in Chapter 3, I provide a summary of the major findings, their relevance for the literature and further steps.

CHAPTER 2

MISSISSIPPI RIVER PLUME VARIABILITY IN THE GULF OF MEXICO FROM SMAP AND MODIS-AQUA OBSERVATIONS

Da Silva and Castelao. Submitted to Journal Geophysical Research: Oceans, May 8, 2018.

Abstract

The Mississippi River is an important source of freshwater and terrigenous material to the Gulf of Mexico. We used sea surface salinity measurements from the Soil Moisture Active Passive (SMAP) satellite and terrigenous dissolved organic carbon (tDOC) from MODIS to describe the Mississippi River Plume (MRP) seasonality and interaction with the Gulf circulation. Our analyses reveal good agreement between SMAP and *in situ* salinity for $S > 31$, and that satellite-derived tDOC can serve as a useful tracer for the river plume. A boundary-detection algorithm was used to quantify the frequency of plume occurrence in the Gulf for the last 15 years. The MRP has its maximum offshore extension during summer, retracting to closer to shore during fall/winter. Variability at monthly time scales is controlled by river discharge and alongshore winds, which explain up to 60% of the local variance in the frequency of plume occurrence near the shelfbreak. Maximum variability in plume extension is found to the east of the Mississippi Delta due to wind reversals that generally occur during summer. The combined use of SMAP salinity and MODIS tDOC allowed for a detailed view of anomalous events in 2015 and 2016, when the MRP was transported for 350 km from the coast due to interactions with the Loop Current and with dipole eddies. While SMAP observations allow for tracking the river plume even in cloudy conditions, high resolution MODIS data allow for a more accurate characterization of sharp fronts and of the width of river-influenced filaments.

Keywords: Mississippi River, river plume, SMAP, tDOC, MODIS-Aqua.

2.1. Introduction

The Mississippi River (MR) is an important source of freshwater and terrigenous material to the Gulf of Mexico (GoM). It is the largest river in North America with an average discharge of 13,500 ± 2,000 m^3 s^{-1} (Hu et al., 2005). The river plays a critical role on the interaction between terrestrial and marine carbon reservoirs, exporting about 3.6 x 10^6 tons of carbon per year (Degens et al., 1991). Highly productive river-influenced waters can support fisheries activity and coral reef diversity on the Louisiana-Texas Shelf (Rabalais et al., 1991), for instance. At the same time these waters contribute to the development of summertime hypoxia in bottom waters (Rabalais et al., 1991, Bianchi et al., 2010). Thus, understanding the Mississippi River plume dynamics and the processes that control its variability is important to better understand its influence on biogeochemical processes in the ocean. Although the Mississippi River is the primary and most expressive source of freshwater waters in the GoM, several other smaller sources of freshwater (e.g., Atchafalaya River, Mobile River) are also important.

Observational data sets and numerical modeling (e.g., Lohrenz et al., 1990; Green et al., 2006; Luo et al., 2016) have been used to describe the MRP (Cochrane and Kelly, 1986; Schroeder et al., 1987). In general, the Mississippi River plume circulation is characterized by westward flow along the Louisiana and Texas Shelf during fall, winter and early spring. The flow is driven primarily by westward winds (Walker 1996; Ohlmann & Niiler, 2005), discharge, and Coriolis force (Dinnel & Wiseman, 1986; Walker 1996). Many observational studies, however, have reported reversions of the MRP to the east of the Mississippi Delta (e.g., Murray, 1972; Walker & Hammack, 2000; Morey et al., 2003b; Walker et al., 2005), which are often related to changes in the wind

direction in the GoM (Walker et al., 2005). In addition, there are reports of Mississippi River-influenced waters reaching the Florida Strait (Walker et al., 1994; Hu et al., 2005) or the Gulf Stream (Ortner et al., 1995; Gilbert et al., 1996). The extension of the MRP until the Florida Strait and Gulf Stream was driven by a combination of factors, such as winds, Loop Current entrainment, and eddies (Wiseman & Dinnel, 1988; Ortner et al., 1995; Gilbert et al., 1996; Morey et al., 2003a; Hu et al., 2005; Schiller et al., 2011; Schiller & Kourafalou, 2014).

Although much has been learned from these studies, *in situ* observations are generally restricted to relatively small areas over short time periods (e.g., shipboard surveys), or provide point measurements over periods of up to a few years (e.g., moorings). Additionally, most *in situ* observations in the northern Gulf of Mexico are focused on the continental shelf. The recent availability of satellite observations of sea surface salinity (SSS) provides a great opportunity to investigate plume variability on large spatial and temporal scales from an observational point of view. Previous studies (Grodsky et al., 2012, 2014; Gierach et al., 2013; Fournier et al., 2015; Chao et al., 2015) have used SSS derived from Soil Moisture Ocean Salinity (SMOS) and/or Aquarius to investigate regions influenced by river plumes (e.g., Amazon, Mississippi, Congo rivers). SSS measurements are also available from the Soil Moisture Active Passive (SMAP) mission, which was launched in 2015 (Entekhabi et al., 2010). The new satellite provides near global coverage with a footprint of 40 km, which is substantially smaller than the 100 km footprint from Aquarius (Dohan et al., 2015). It is also less sensitive to Radio Frequency Interference than SMOS satellite (see supplementary information in Fournier et al., 2016).

Several recent studies (Fore et al., 2016; Fournier et al., 2016, 2017; Tang et al., 2017) have compared SMAP SSS observations with *in situ* measurements. Tang et al. (2017) compared SMAP SSS on a global scale with *in situ* measurements from ARGO floats, moored buoys and ship-based thermosalinograph. They showed that SMAP provides reliable measurements between 40^{o} N and 40^{o} S, and they were able to track large salinity changes that occurred on month time scale. Fournier et al. (2016) demonstrated that SSS derived from SMAP compares better with *in situ* data from coastal regions in the Gulf of Mexico than SSS from SMOS. SMAP has also been shown to capture the strong horizontal SSS gradient during a post monsoon season in the Bay of Bengals (Fournier et al., 2017). In summary, these studies provided the first indications of the success of SMAP for tracking river plumes in coastal regions through their SSS signature. However, the implications of the relatively low resolution of SMAP data to characterize sharp fronts and the small spatial scales of variability that are generally observed in the coastal ocean have not been fully investigated.

Ocean color can also provide useful information about the distribution of river-influenced waters in coastal systems. Several studies have used satellite-derived chlorophyll measurements to investigate river plume variability (e.g., Del Castillo et al., 2001; Walker et al., 2005; Molleri et al., 2010). The underlining assumption is that nutrient input from the river will result in enhanced phytoplankton biomass, so that river-influenced water will be relatively enriched in chlorophyll. However, inputs of nutrient from other sources (e.g., upwelling) can also lead to chlorophyll enhancement. Thus, Chl-a may not always be an effective tracer for river plumes due to the influence of marine and terrestrial sources. Therefore, it is useful to focus on a proxy that has only terrigenous

sources. Helms et al. (2008) demonstrated that the spectral slope coefficient of chromophoric dissolved organic matter (CDOM) absorbance between 275 and 295 nm ($S_{275\text{-}295}$) is a reliable optical tracer for terrigenous dissolved organic carbon (tDOC). One of the main components of tDOC is lignin, a class of organic polymers unique to land vascular plants that has no sources in the marine environment (Sarkanen & Ludwig, 1971; Opsahl & Benner, 1997). Thus, tDOC can be used as a tracer of river plumes because its main component is strictly derived from land (Hedges & Parker, 1976).

Recently, Fichot et al. (2013; 2014) developed an algorithm based on remote-sensing reflectance (Rrs) data from the Moderate Resolution Imaging Spectroradiometer (MODIS-Aqua), providing high-resolution observations since 2002. The algorithm uses multiple Rrs bands to estimate the spectral slope coefficient of CDOM absorbance from satellite ocean color data. Fichot et al., (2014) showed that $S_{275\text{-}295}$ estimated based on satellite data agrees with *in situ* $S_{275\text{-}295}$ measurements, with an average uncertainty of 10%. As mentioned above, $S_{275\text{-}295}$ is a tracer of tDOC in river influenced ocean margins and is therefore tightly linked to continental runoff distributions (Helms et al., 2008; Fichot & Benner, 2012; Medeiros et al., 2017). Fichot et al. (2014) used a non-linear regression to model the relationship between $S_{275\text{-}295}$ and tDOC concentration and thus derive an algorithm to estimate tDOC concentration from ocean color. This provides a way to obtain multi-year, high-resolution satellite-derived measurements of a quantity that is tightly coupled to the distribution of riverine water in the ocean. The algorithm was developed and calibrated using data from the northern GoM, including from regions under the influence of the MRP.

Both data sets present limitations, with SMAP being of comparatively low resolution and covering a relatively short time period (which does not allow for a seasonal description of the MRP) and MODIS-Aqua being an indirect tracer for the plume and being affected by cloud coverage. Thus, we used a combination of SMAP and ocean color data to obtain a comprehensive description of plume variability. Specifically, this study aims to 1) describe the variability of the Mississippi River plume in the GoM based on decade-long satellite observations, to 2) identify the main forcing mechanisms that drive the MRP spreading in the ocean, and to 3) evaluate the use of SMAP SSS and MODIS tDOC to describe the MRP.

2.2.Methods

Remote Sensing Data

Terrigenous dissolved organic carbon

Daily remote sense reflectance (Rrs) data from MODIS-*Aqua* (oceandata.sci.gsfc.nasa.gov/MODIS-Aqua) with 4 km resolution are used to estimate terrigenous dissolved organic carbon (tDOC) concentration based on the Fichot et al. (2014) algorithm. The tDOC-algorithm was implemented using multiple wavelength bands of Rrs data (443, 488, 555, 667 and 678 nm). The data set used extends from July 2002 to September 2016.

Sea Surface Salinity

The SMAP sea surface salinity (SSS) product used in this study is the radiometer-based, 0.25° resolution and 8-day running average time window level 3, version 2.0 data

set. The near-polar orbit of SMAP allows for complete global coverage of the oceans in 3 days with a repeat cycle of 8 days (Meissner & Wentz, 2016). Although it is difficult to achieve the accuracy of Aquarius's SSS using SMAP measurements (the mission was designed for land applications; Durack et al., 2016), SMAP provides better spatial resolution with a footprint size of about 40 km, which is an advantage for coastal applications. SMAP observations can be obtained in cloudy conditions. The SSS gridded product is produced by the Jet Propulsion Laboratory (https://smap.jpl.nasa.gov/) based on retrieval algorithm modified from that used for Aquarius SSS retrieval (Yueh et al., 2013, 2014; Fournier et al., 2016). The data set is available since April 2015.

Plume Boundary

One of our main objectives is to use the long-term MODIS data set to identify regions in the northern Gulf of Mexico that are influenced by the river plume. In order to define the plume boundary, an algorithm able to differentiate noisy fluctuations from the actual plume signature is required. Many edge-detection algorithms have been developed and implemented for oceanographic purposes, either based on gradients (e.g., Canny, 1987) or on data distribution (e.g., Cayula & Cornillon, 1992). The main goal of theses algorithms is to detect regions of strong gradients (i.e., fronts). However, our goal is not to identify the regions with strongest gradient, but rather the offshore boundary of the river plume. Since the strongest gradient across the plume front is generally located several kilometers inshore of the plume boundary, using preexistent algorithms underestimate the MRP area.

Examination of 9-day running means of the MODIS data reveals that tDOC generally decreases monotonically as a function of distance from the coast, which is consistent with previous studies based on *in situ* data (Benner & Opsahl, 2001). We found that the tDOC concentration is generally characterized by two plateaus (one near the coast and one farther offshore) separated by an abrupt decay as the distance from the coast increases. This behavior can be well represented by a sigmoid curve. The plume boundary-detection algorithm is thus based on fitting a logistic (sigmoid) curve to the tDOC data as a function of distance from the coast. Because of extensive cloud coverage, monthly data are used. In the fit

$$f(x) = \alpha + \frac{(\beta-\alpha)}{1+ e^{-\gamma(x-\delta)}} \qquad \text{(Eq. 1)}$$

α is the minimum value of the tDOC concentration, β is the difference between the maximum and the minimum concentration, γ (= 10) is the slope of the curve (estimated based on the observations), δ is the point of half decay, and x is the distance from the coast. For each longitude, α, β and δ change iteratively. The value of α for each fitted function is then used to calculate the mean plus two standard deviations for the entire period, which is then used as a threshold to identify the plume boundary. It can be interpreted as the minimum concentration of tDOC in the region, or as the background concentration of tDOC in the northern Gulf of Mexico, without the influence of the river plume. Using this procedure, the threshold value identified is larger than the individual values of α for 97.5% of the fits. Using this conservative approach, we define regions with tDOC concentration larger than the threshold as the river plume. Visual inspections for all months between July 2002 and September 2016 indicate that the algorithm is able to efficiently capture the plume boundary, including the presence of narrow filaments

(Figure 2.1). We have also tested the algorithm in another coastal setting (Columbia River plume off the U.S. West Coast) with great success, indicating that it is robust against noisy data.

Plume frequency of occurrence and area

Because of large spatial and seasonal differences in cloud cover, comparisons of plume distribution between different regions and time periods are often difficult because each region is, in general, sampled at different times. To account for that, we divide the number of times a pixel qualifies as river plume by the total number of months for that pixel during the study period, yielding a frequency of plume occurrence. For each month, we also estimate the plume area to quantify the extension of the MR plume in the Gulf of Mexico. Empirical orthogonal function (EOF) decompositions of tDOC concentration and of the frequency of plume occurrence are used to identify the dominant modes of variability in the system, following Overland and Preisendorfer (1982) to determine the modes that are significant.

In situ Salinity

We used *in situ* salinity data from a flow-through system from 8 research cruises (Table 2.1) to evaluate tDOC as a proxy for the river plume and to compare with SMAP SSS measurements. It is important to note that the satellite measures salinity at the top few centimeters of the ocean (Entekhabi et al., 2010). In contrast, *in situ* salinity was measured at 4 m depth. In times of significant near-surface salinity stratification (e.g., due to the presence of thin freshwater lenses), the difference in sampling depth can

contribute to differences between SMAP and *in situ* salinity observations (Boutin et al., 2016).

River Discharge

The discharge data was derived from the United States Geological Survey (USGS). We used two different data sets to reconstruct the entire monthly discharge time series from January 2002 to September 2016. The first data set, Streamflow and Nutrient Flux of Mississippi-Atchafalaya River Basin and Sub basins through Water year 2015, covers the period from January 2002 to September 2015 (https://toxics.usgs.gov/hypoxia/mississippi/flux_ests/delivery/index.html). The second, Station Mississippi River at Belle Chase, LA, covers the period from November 2008 to March 2017. Data from this second time series are used to extend the river discharge time series via a linear regression.

Wind

The Cross-Calibrated Multi-Platform (CCMP) version 2.0 (http://www.remss.com/measurements/ccmp/) gridded surface vector winds are produced using a combination of the Version-7 RRS radiometer wind speed, QuikSCAT and ASCAT scatterometer wind vectors, moored-buoy wind data, and ERA-Interim model wind field using a variational analysis method (Atlas et al., 2011). The product is available since July 1987 at 0.25° resolution.

Drifter

A drifter drogued at 1 m below the surface (Davis, 1985) was deployed on July 22nd, 2015 at 27.53° N and 90.6° W, providing observations until August 4th, 2015. The drifter trajectory is publicly available at the Northeast Fisheries Science Center, NOAA Fisheries Service (https://www.nefsc.noaa.gov/drifter/index_2015.html).

Surface currents

Surface geostrophic velocities were derived from delayed mapped absolute dynamic topographic (MADT-UV) produced by Archiving, Validation, and Interpretation of Satellite Oceanographic (AVISO, http://www.aviso.altimetry.fr) at 0.25° of resolution.

2.3.Results

Comparison between *in situ* salinity and satellite-derived SSS and tDOC

Comparisons between *in situ* observations and satellite data are often challenging, in part because of the large footprint of the satellite data compared with *in situ* point measurements. Despite that, comparisons between *in situ* salinity from eight research cruises (Table 2.1.) and satellite-derived estimates of tDOC reveal that they are negatively correlated to each other ($r = -0.58$; Figure 2.2a). This relation is expected, since sources of tDOC are exclusively terrigenous, and consistent with Benner and Opsahl (2001) results. We note that although satellite-derived tDOC and *in situ* salinity are related to each other, there is a substantial amount of scatter in the relationship (Figure 2.2a).

Since the recent launch of SMAP, studies have characterized SSS uncertainties in the coastal ocean (e.g., Fore et al., 2016; Fournier et al., 2016) and the importance of near-surface salinity stratification that can develop under low wind speed conditions on validation efforts (Boutin et al., 2016). Our results show that salinity derived from SMAP is in good agreement with *in situ* salinity (r =0.75, Figure 2.2b). There is a better agreement for salinities greater than 31, suggesting that SMAP provides a better representation of salinity off the shelf in the northern GoM. For regions closer to the coast with S < 31, the analysis reveals that SMAP overestimates salinity compared to *in situ* data, possibly due to the smaller scale of variability of coastal processes. In addition, the differences between SMAP SSS and *in situ* salinity present larger variability close to the coast decreasing with increasing distance from shore (Figure 2.2c), although the mean bias remain small except very near the coast.

Salinity data derived from sparse CTD casts have provided insightful information about the quality of SMAP SSS (e.g., Fournier et al., 2016). However, they do not allow for spatial scales resolved by SMAP to be identified (e.g., smoothing of SSS fronts). Salinity data derived from flow-through system, on the other hand, allows for identifying salinity fronts and for comparisons with fronts identified based on tDOC and SSS derived from SMAP. Two examples of salinity fronts that were detected near the Mississippi Delta using *in situ* data in May and June 2015 are shown in Figure 2.3. While the front observed in May (Figure 2.3a) around km 190 is 22 km wide based on *in situ* observations (which is narrower than the footprint of SMAP), it is about 65 km wide based on SMAP data. In June 2015 (Figure 2.3b), the coastal region influenced by low-salinity waters is approximately 100 km wide, with *in situ* salinity being approximately

uniform offshore of that. SMAP observations reveal a weaker SSS gradient for 300 km. Thus, both fronts are clearly captured with SMAP data, although they are smoothed compared to the *in situ* data.

The fronts observed in May based on *in situ* data (at km 190, 445 and 480) are also captured by tDOC data (Figure 2.3a). In that case, the widths of the fronts are in better agreement with the *in situ* data than when fronts are identified in SMAP. This suggests that, although not providing a direct measurement of salinity, MODIS-derived tDOC data can provide useful information about scales of variability in the coastal ocean, including the width of salinity fronts associated with river plumes. Cloudy conditions prevented the observation of the front in June 2015 using tDOC data (Figure 2.3b). These demonstrate some of the advantages and disadvantages of the different satellite data sets, illustrating the usefulness of a combination of SMAP SSS and MODIS tDOC to describe the river plume.

Mississippi River Plume Variability

The dominant modes of variability of the MRP were determined through an EOF decomposition of the monthly data of tDOC concentration and frequency of plume occurrence. The mean patterns for the respective variables are shown in Figure 2.4, revealing the mean distribution of the river plume in the northern Gulf of Mexico.

The dominant EOF of tDOC concentration explains 37.6% of the total variance (Figure 2.5a) and 40-60% of the local variance over the shelf (Figure 2.5b). Large EOF values are restricted to the continental shelf extending for a large distance (>500 km) along the coast to the west of the Mississippi Delta, but to a much shorter distance (< 200

km) along the coast to the east of the delta. The increase in tDOC concentration generally occurs from March to July and decays from August to November (Figure 2.5c), although significantly interannual variability is observed (Figure 2.5d). The observed pattern is correlated with river discharge ($r = 0.72$) with a time lag of 23 days. If the seasonal cycle is first removed from both time series, the correlation coefficient decreases slightly to 0.70 with a lag of 16 days. In both cases the correlation coefficients are statistically significant at the 95% confidence level. Note that the amplitude time series of the dominant EOF of tDOC concentration is smaller from July 2005 to December 2006 compared to the other years, likely because of the lower-than-average river discharge during that period (Figure 2.5d).

Our analysis reveals that the continental shelf is under the influence of the MRP over the entire year (frequency of plume occurrence of 100%; Figure 2.6). However, there are periods (e.g., summer) when the plume extends beyond the shelfbreak. The offshore movement of the plume begins in June peaking in August, while the plume retreats in September. It is possible to observe that the east side (90°W – 85°W) of the Mississippi Delta presents the greatest variability of the plume frequency (Figure 2.6 and Figure A1), reaching up to 50-60% beyond the 100 m isobath during summer. Variability to the west of the Mississippi Delta (95°W – 90°W) is substantially smaller, with maximum frequency around the 100 m isobath during summer at 10-20%.

The dominant EOF of the frequency of plume occurrence explains 23.2% of the total variance, with large values being observed around the 100 m isobath (Figure 2.7a) near the average location of the offshore boundary of the plume (Figure 2.4b). Near the coast the EOF approaches zero, since that region is under the influence of the river plume

100% of the time (see Figure 2.6). The frequency of plume occurrence increases near the shelfbreak during June to August peaking in July and decreases from September to December (Figure 2.7c). This indicates that the plume extends farther offshore during summer, while it retreats to closer to shore later in the year during fall. The same pattern can be observed in each individual year (Figure 2.7d), except from July 2005 to December 2006 when river discharge was anomalously small. The mode explains a larger fraction of the local variance to the east of the delta (89-86°W), ranging between 50 and 60%. The amplitude time series of EOF 1 of the frequency of plume occurrence and river discharge are significantly correlated ($r = 0.52$) with a lag of 25 days. The correlation coefficient decreases to 0.48 with a lag of 24 days if the respective seasonal cycles are removed from both time series, indicating that river discharge plays an important role controlling the width of the plume. Indeed, tDOC concentrations on the continental slope just offshore of the river delta have been shown to be correlated with river discharge on an annual scale (Fichot et al., 2014).

Alongshore winds have long been known to drive cross-shelf displacements of plume boundaries (e.g., Fong & Geyer, 2001; Lentz, 2004). In order to quantify the effects of alongshore winds, we selected two regions where variability in the frequency of plume occurrence is large (Figure 2.7a), one to the west (Box West) and one to the east (Box East) of the Mississippi Delta. Although winds are predominantly downwelling favorable for most of the year, average winds become weaker or even reverse to weakly upwelling favorable during summer (Figures 2.8a and c). Monthly-averaged alongshore winds were upwelling favorable for 25 of the 171 months analyzed here for Box West, while they were upwelling favorable for 49 months on Box East. This indicates that summertime

winds tend to be more upwelling favorable to the east compared to the west of the delta. The strongest correlation between alongshore winds in Box West and Box East and the amplitude time series of EOF 1 of frequency of plume occurrence occurs for relatively small lags, 3 and 7 days. The correlation coefficients are 0.51 (Box West, Figure 2.9a) and 0.52 (Box East, Figure 2.9b), consistent with upwelling favorable winds resulting in a wider plume. When the seasonal cycle is removed, correlation coefficients decrease to 0.36 (Box West) and 0.29 (Box East), but they are still statistically significant (95 % confidence level). It is interesting to note that for low values of EOF 1 (< –0.05), which indicate times when the plume is narrow, the correlation between winds and the amplitude time series seems to be weaker (i.e., amplitude of EOF remains unchanged for monthly-averaged downwelling winds stronger – more negative – than 0.04 Pa; Figure 2.9). Although it is not clear if this pattern is significant due to the small number of events, it could indicate a limit for which stronger downwelling favorable winds would not cause further onshore transport of the plume boundary.

Plume Area

Time series of the MRP area and its monthly averages (Figure 2.10) present a similar pattern to those observed for the dominant EOF of the frequency of plume occurrence (Figure 2.7c, d). This suggest that the onshore/offshore movement of the plume boundary captured in the EOF analysis is the main factor controlling the MRP area. As such, the MRP area is primarily controlled by alongshore winds and river discharge.

The maximum area of the MRP generally occurs during summer (Figure 2.10) peaking in July (1.12×10^5 km^2 $\pm$ 0.09×10^5 km^2), which is consistent with the seasonality

of the MRP described in the previous sections. The minimum area occurs during fall in October (0.79×10^5 km^2 ± 0.09×10^5 km^2). The time series reveals several events of interannual variability, with anomalously large areas occurring in March 2010, in July 2015, 2009, 2008, 2011 and in August 2013. During those months, the plume area was 1.11-1.69 times larger than the long-term average for the respective month. The time series also reveals the interplay between river discharge and wind forcing on the control of plume distribution. The plume area was anomalously high in 2008 and 2011, for example. The Mississippi River basin experienced intense rainfall in March-April 2008 (Shi & Wang, 2009), which resulted in a 40% increase in river discharge compared to average conditions (Figure 2.5d). In addition, we observed in our analyses three Loop Current eddies interacted with the river plume during this period (not shown). In 2011, the region also experienced strong rainfall (Androulidakis & Kourafalou, 2013) resulting in the largest MR discharge during the study period (45,000 $m^3.s^{-1}$, Figure 2.5d). In the years with the largest plume areas, 2010 and 2015, upwelling-favorable winds were stronger than average and river discharge was also anomalously high. During the summer months in 2005, 2006, 2007 and 2012, on the other hand, the plume area anomalously low (Figure 2.10). Summertime winds were more downwelling-favorable than average in those year (Figure 2.8), which presumably contributed to maintaining the MRP close to the coast.

Anomalous events

The long-time series of satellite-derived tDOC spanning almost 15 years allows for identifying anomalous events in which plume waters were transported far offshore. For

that, we analyzed Hovmöller diagrams of tDOC concentration anomaly (i.e., removing the seasonal cycle) along the 5 bands shown in Figure 2.4b. The 5 bands are located at an average distance of 140, 195, 250, 305 and 360 km from the coast. The largest events of offshore transport of plume waters were observed in the summers of 2009, 2015 and 2016, when the MRP extended for 365 km offshore (Figure 2.11e), and in 2013 when the plume extended about 300 km offshore (Figure 2.11d). In all cases, strongest anomalies indicative of strong cross-shelf transport are generally observed between 92° and 88°W, indicating a preferred region for offshore export of river-influenced waters in the northern Gulf of Mexico.

To better understand the evolution of these strong events of offshore transport, we investigate their progression based on 9-day averages of tDOC concentration from MODIS and 8-day means of sea surface salinity from SMAP, overlaid with geostrophic velocities from altimetry. We focused on the 2015 and 2016 events because they are some of the most extensive (Figure 2.11) and because SMAP data are available for those periods (since the satellite was launched in early 2015). The evolution of the MRP at selected dates from 12 July to 6 September, 2015 is shown in Figure 2.12, while the evolution from 11 July to 2 September, 2016 is shown in Figure 2.13. Satellite images for all days in those two time periods are shown in Appendix A, Figures A2-5.

The 2015 event, which has been described in detail by Fournier et al. (2016), was characterized by anomalously large river discharge (1.3 times larger than the average for July), a northward position of the Loop Current, and the passage of a large anticyclonic eddy. These contributed to transport low salinity, high tDOC water offshore forming a horseshoe shape (Figure 2.12). Note that the offshore transport of low-salinity water in

late July at 91ºW captured by SMAP closely matches the surface current speed as measured by the surface drifter.

Although the offshore transport of river-influenced waters can be observed with both data sets, cloud coverage was substantial creating extensive gaps in the MODIS data set. During cloud-free periods, however, the spatial scales of the features resolved by the data sets are quite different. Analysis along the transect shown in Figure 2.12 for 26 August 2015 reveals a filament of river-influenced waters that is about 100 km wide based on MODIS tDOC data, but much wider (~250 km) based on SMAP SSS. This is consistent with the comparison between MODIS-tDOC/SMAP-SSS and *in situ* observations previously described (Figure 2.3).

In 2016, strong offshore transport of riverine water was associated with the presence of two large eddies with opposite polarity in the GoM (Figure 2.13). Although the offshore transport of the plume was also captured by SMAP (Figure 2.13), the filament was considerably wider (180 km) compared to the width estimated using MODIS (93 km) (Figure 2.14b). It is also possible to observe water with high tDOC content being transported along the boundary of the cyclonic eddy on 17 and 25 August (Figure 2.13), creating an isolated pool of oceanic water with low tDOC content in the eddy interior (Figure 2.14c, d). The transport of riverine-influenced waters around the cyclonic eddy on August 17-25 was not fully captured by SMAP (Figure 2.13). As a result, the pool of oceanic water present at the center of the eddy identified with MODIS data is not identifiable with SMAP (Figure 2.14c, d). This again points to the different spatial scales that can be resolved with the different data sets.

2.4.Discussion

Satellite-derived measurements of sea surface salinity (SSS) from SMAP and terrigenous dissolved organic carbon (tDOC) from MODIS were used to describe the Mississippi River plume (MRP) variability in the northern Gulf of Mexico, as well as to identify the main forcing mechanisms controlling plume distribution. The use of MODIS-tDOC as a tracer of the river plume is particularly useful because of the long-term availability of data spanning over 15 years. In combination with the use of a boundary-detection algorithm, this allowed us to estimate for the first time the frequency of plume occurrence at each location in the northern Gulf, building on a number of previous studies that used a similar approach to characterize sea surface temperature frontal variability in coastal systems (e.g., Moore et al., 1997; Mavor & Bisagni, 2001; Miller, 2004; Kostianoy et al., 2004; Castelao et al., 2006; Belkin & O'Reilly, 2009). Quantifying the frequency of plume occurrence is important because it helps identify how often a given region is influenced by riverine waters (and any material it contains, including nutrients, carbon, contaminants) on a monthly time scale.

The analyses reveal that the MRP variability is characterized by (1) predominant extension along the Louisiana-Texas (LATEX) shelf throughout the year (2) with reversals during summer, when the MRP extends farther east; (3) stronger variability to the east of the Mississippi Delta compared to regions to the west of the Delta, and (4) offshore extension during the summer and retraction during fall. This is consistent with previous studies based on moorings and numerical models (e.g., Morey et al., 2003b; Nowlin et al., 2005) that revealed the influence of downwelling-favorable winds from fall to late spring generating wind-driven coastal currents that advect most of the MR waters

onto the LATEX shelf (Walker & Hammack, 2000). During summer, upwelling favorable winds are more common to the east of the Mississippi Delta favoring eastward (Cochrane & Kelly, 1986; Walker et al., 2005) and offshore transport of the MR plume (Morey et al., 2003b; and Schiller et al., 2011).

Several studies (e.g., Fong & Geyer, 2001; Lentz, 2004; Whitney & Garvine, 2005; Castelao et al., 2008; Jurisa & Chant, 2013) have shown that winds play an important role in river plume transport via Ekman dynamics. Our analyses reveal that both river discharge and alongshore winds are the dominant mechanisms controlling the width of the plume on monthly time scales, explaining up to 60% of the local variance in plume frequency variability near the shelf break. While plume variability responds to river discharge on a time scale of a few weeks, the response to wind forcing occurs on shorter time frames of 3-7 days. The response to wind forcing seems to be asymmetric: while upwelling favorable winds result in a progressive increase in plume width (Fong & Geyer, 2001; Lentz, 2004), the opposite may not be true for downwelling favorable winds. Weak downwelling winds lead to a narrowing of the plume. However, strong downwelling winds may not result in further narrowing of the plume, presumably because of the opposing pressure gradient. Is not clear if this result is significant considering the relatively small number of months with strong downwelling winds on average. It will be interesting to identify if this pattern will hold as additional MODIS data are gathered.

The use of satellite observations spanning multiple years also allowed for the first quantitative estimate of the seasonal variability in MRP area to be obtained (Figure 2.10). The seasonality of the MRP area reflects the influence of the wind field and river

discharge. In March 2010, strong upwelling-favorable winds and high river discharge were responsible for the largest area of the MRP observed during the study period. Increases in plume area can have large chemical and biological implications. The large area of the plume in March 2010 was correlated with reduced partial pressure of carbon dioxide (pCO_2), and the wider plume was a stronger CO_2 sink by a factor of five when compared to more typical plume conditions (Huang et al., 2013). There were other instances in which the plume area was only slightly smaller than in March 2010 (Figure 2.10), indicating the potential for strong air-sea CO_2 fluxes during those periods (Huang et al., 2013). Periods with anomalously small plume area (e.g., 2005, 2006, 2007 and 2012) associated with predominantly downwelling-favorable winds and low river discharge will also presumably impact biological and chemical processes, including air-sea CO_2 fluxes.

On time scales shorter than one month, such as those observed during the 2015 and 2016 events shown here, interactions with the Loop Current (LC) and offshore eddies play a critical role driving the plume offshore (Ortner et al., 1995; Hu et al., 2005; Walker et al., 2005; Schiller et al., 2011; Schiller & Kourafalou, 2014; Fournier et al., 2016, 2017). Those pulses of offshore transport of plume water are characterized by strong interannual variability (Fichot et al., 2014). As the low-salinity water is rapidly transported offshore, strong salinity fronts are formed (Figure 2.14).

SMAP and MODIS-Aqua

Unlike other variables (e.g., temperature, sea surface height, ocean winds), high quality satellite observations of sea surface salinity (SSS) only became available recently

with the Aquarius platform (Lagerloef et al., 2008; see also special section of Journal of Geophysical Research in 2014). Because of Aquarius' large footprint, however, studies of river plume distribution in the coastal ocean, where scales of variability are generally reduced compared to the open ocean, remained challenging. Recent studies have demonstrated the usefulness of NASA's Soil Moisture Active-Passive (SMAP) satellite (Meissner & Wentz, 2016) to investigate salinity variability in the coastal ocean (Fournier et al., 2016, 2017; Tang et al., 2017). Specifically, SMAP provides better spatial resolution with a footprint size of about 40 km, which is an advantage for coastal applications.

In addition to not being influenced by clouds, an obvious advantage in regions with high cloud coverage, SMAP measures salinity which is directly related to the river plume. Our results show that SMAP data are in good agreement with *in situ* measurements for salinities larger than ~31, with SMAP being slightly fresher than *in situ* data (Fournier et al., 2016). It is possible that some of these differences are related to salinity stratification, since the *in situ* measurements were obtained 4 m below the surface. The mismatch between the two data sets increases for salinities lower than about 30-31, however, with SMAP salinity being larger than *in situ* data. Comparisons with *in situ* flow-through data collected during several research cruises reveal that SMAP observations substantially smooth salinity gradients and as such overestimate the width of fronts because of its relatively low resolution. This is expected, since its footprint is larger than the width of most fronts in the coastal ocean. Front width estimated from SMAP data can be up to 3 times larger than the width obtained from *in situ* data. High resolution MODIS-tDOC data, on the other hand, do a remarkable job capturing the

location and width of salinity fronts in the northern Gulf of Mexico, comparable to *in situ* observations. It also provides observations much closer to shore (where the strongest river plume signature is found) compared to SMAP. As such, MODIS can provide useful information about sharp fronts and small-scale features that would be otherwise missed.

The long-time series (15+ years) of MODIS-tDOC allows for robust characterization of the seasonality and interannual variability in plume variability and interactions with the GoM circulation. However, clouds impact the visualization of the data on short time scales, and thus the investigation of specific events can be difficult even when 9-day averages are used (Figure 2.12 and 2.13). Despite that, we found that tDOC can be used as an efficient tracer for the river plume due its terrigenous origin characteristic. Preliminary tests for the Columbia River plume region indicate good agreement with salinity, indicating that it can be a powerful complementary tool to identify the distribution of river plumes from satellites. Lastly, MODIS-Aqua can be used to characterize plume distribution and variability in high latitude regions. This is important, because significant biases in SMAP SSS are observed in latitudes higher than 40° (Meissner & Wentz, 2016) because L-band radiometers (i.e., Aquarius, SMAP) have poor sensitivity to salinity in high-latitudes (Durack et al., 2016).

Collectively, our analyses demonstrate the advantages of combining the use of SMAP SSS and MODIS-tDOC to characterize river plume distribution and variability. While SMAP data are not influenced by clouds and provide a direct measure of salinity, the high-resolution data from MODIS provides a good representation of sharp fronts and other small-scale features that are typical of coastal ocean processes.

2.5.Conclusion

The use of satellite-derived SSS and tDOC as a riverine proxy allowed us to describe the seasonality and large-scale features of the MRP with an unprecedented level of detail. Our results show that the MRP tends to extend farther offshore during summer when the region is influenced by upwelling-favorable winds and to retreat to closer to the coast during fall and early winter, when predominant winds are downwelling-favorable. The eastern portion of the Mississippi Delta presents the greatest variability of the MRP extension during the year. Our novel approach of quantifying the frequency of plume occurrence identified the regions and time periods in which the northern Gulf of Mexico is more strongly influenced by riverine waters. Up to 60% of the variance in plume distribution near the shelf break on monthly time scales is associated with wind forcing and river discharge. On shorter time scales, interactions with the Loop Current and associated eddies play a critical role transporting the MRP offshore. Our findings contribute to the understanding of the river plume seasonality and its interaction with winds and the large-scale circulation in the GoM.

The combined use of SMAP SSS and MODIS tDOC data proved to be a powerful tool to investigate the dynamics of river plumes, allowing for tracking plume distribution during cloudy periods and to identify sharp fronts and small-scale features that are important in the coastal ocean. This demonstrates the promise for application of the methods used in this study to other regions influenced by riverine waters and will hopefully stimulate comparisons with other basins where offshore boundary currents interact with river plumes.

2.6.Acknowledgements

This research was made possible in part by a grant from The Gulf of Mexico Research Initiative to support the "Ecosystem Impacts of Oil and Gas in the Gulf (ECOGIG)" research consortium, and in part by NASA Ocean Vector Winds Science Team (NNX14AM70G) and Ocean Surface Topography Science Team (NNX13AD80G). Data are publicly available through the Gulf of Mexico Research Initiative Information & Data Cooperative (GRIIDC) at https://data.gulfresearchinitiative.org (doi: 10.7266/N74X565K, 10.7266/N78K77H1, 10.7266/N74X5661, 10.7266/N79P301P, 10.7266/N7NS0S8B, 10.7266/N7154FGM, 10.7266/N72R3Q2B; and 10.7266/N73X84P9). The MODIS-Aqua and SMAP are available at oceandata.sci.gsfc.nasa.gov/MODIS-Aqua and https://smap.jpl.nasa.gov/, respectively. The river discharge, drifter, CCMP v2.0 wind, and Surface currents data are publicly available at https://nwis.waterdata.usgs.gov/, https://www.nefsc.noaa.gov/drifter/index_2015.html, http://www.remss.com/measurements/ccmp/, http://www.aviso.altimetry.fr, respectively. The authors would like to thank the crews of the R/V Endeavor, R/V Point Sur and R/V Pelican for the highly successful field operations. We would like to thank Matheus M. Pacheco for the development of the threshold analysis of the MRP, support on statistics, and the valuable feedbacks in previous versions of the paper. This is ECOGIG contribution no. 509.

Tables

Table 2.1. Research Cruises (https://ecogig.org)

Year	Cruise	Date
2015	R/V Endeavor EN559	May 29th – June 21st
	R/V Point Sur DP02	August 8-22nd
	R/V Point Sur PS16-09	September 14-19th
	R/V Point Sur PS16-18	December 8 – 10th
2016	R/V Pelican PE16-17	March 2 – 6th
	R/V Pelican PE16-20	April 26th – May 3rd
	R/V Endeavor EN586	July 21st – August 14th
	R/V Point Sur PS17-08	October 5 – 9th

Figures

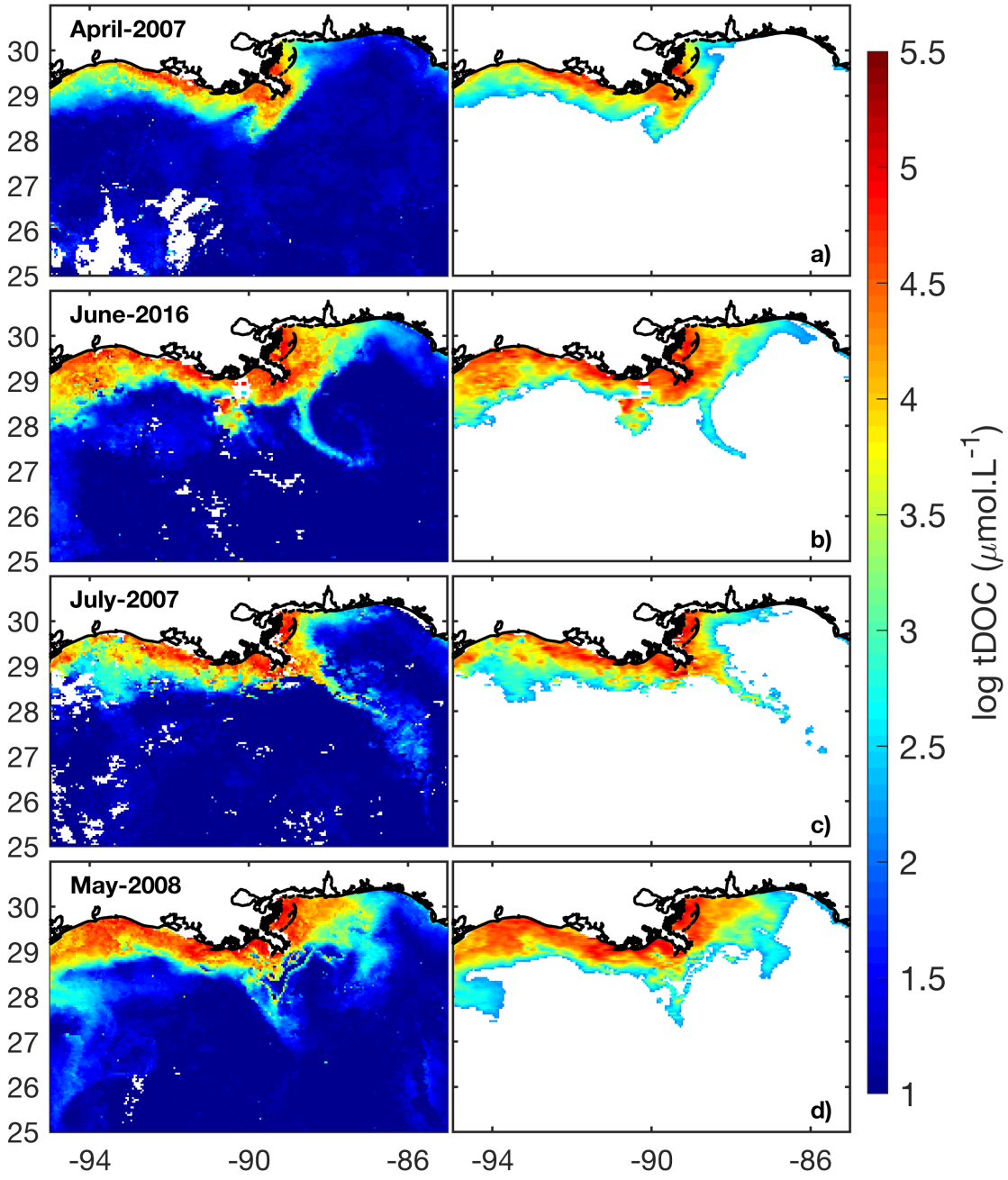

Figure 2.1. (left) mean tDOC concentrations (colors) in the northern Gulf of Mexico for four different months. (right) River plume boundary determined by the boundary-detection algorithm.

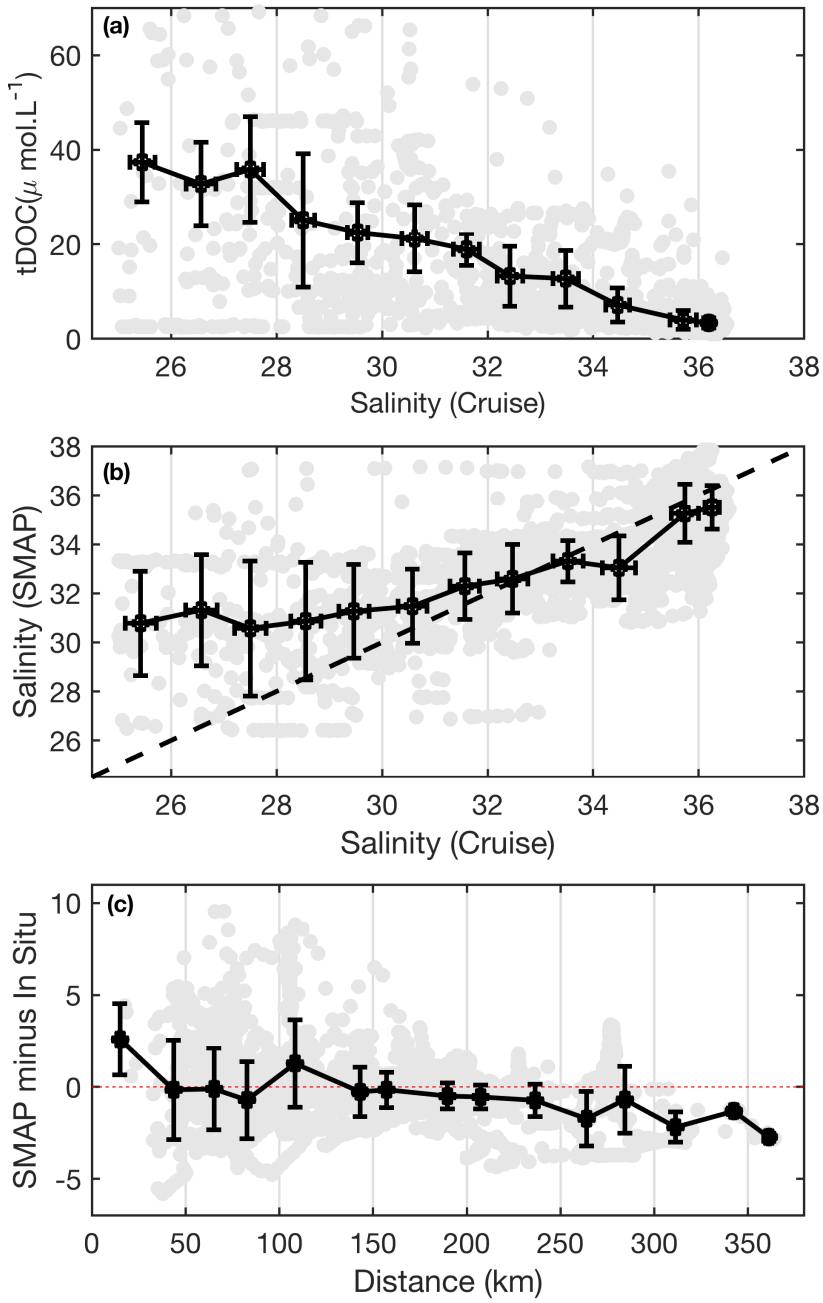

Figure 2.2. (a) Binned scatterplots between tDOC and *in situ* salinity from eight research cruises. (b) Binned scatterplots between SMAP and *in situ* salinity. Dashed black line shows the 1:1 line. (c) Binned scatterplots of SMAP minus *in situ* salinity from eight research cruises versus distance from the coast (km). The light gray dots are the original data.

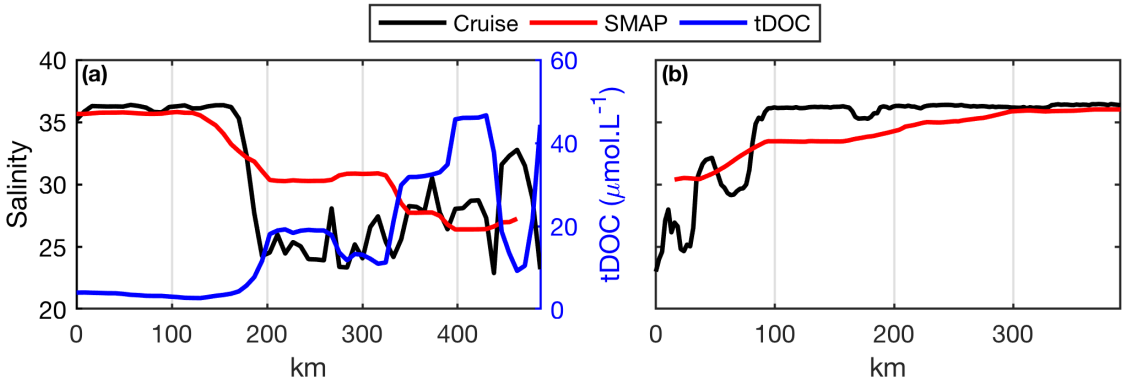

Figure 2.3. Fronts detected by SMAP SSS (red solid line), *in situ* salinity (black solid line) and by tDOC (blue solid line) in May (a) and June (b) of 2015.

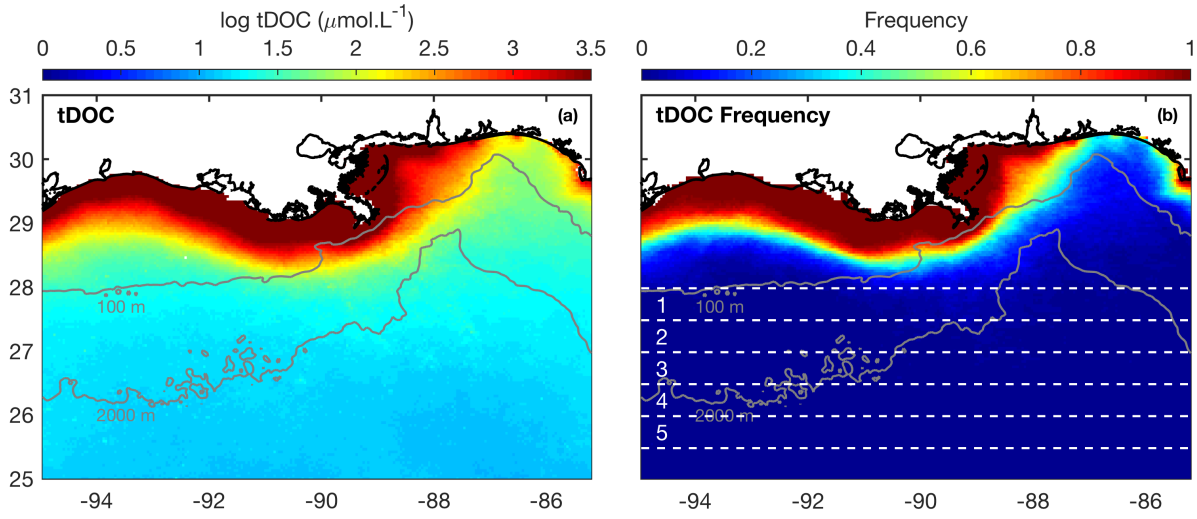

Figure 2.4. (a) Long-term average of (a) tDOC concentration and of the b) frequency of plume occurrence in the northern Gulf of Mexico. The dashed white lines represent the five bands used to compute Hovmöller diagrams (see Figure 2.11).

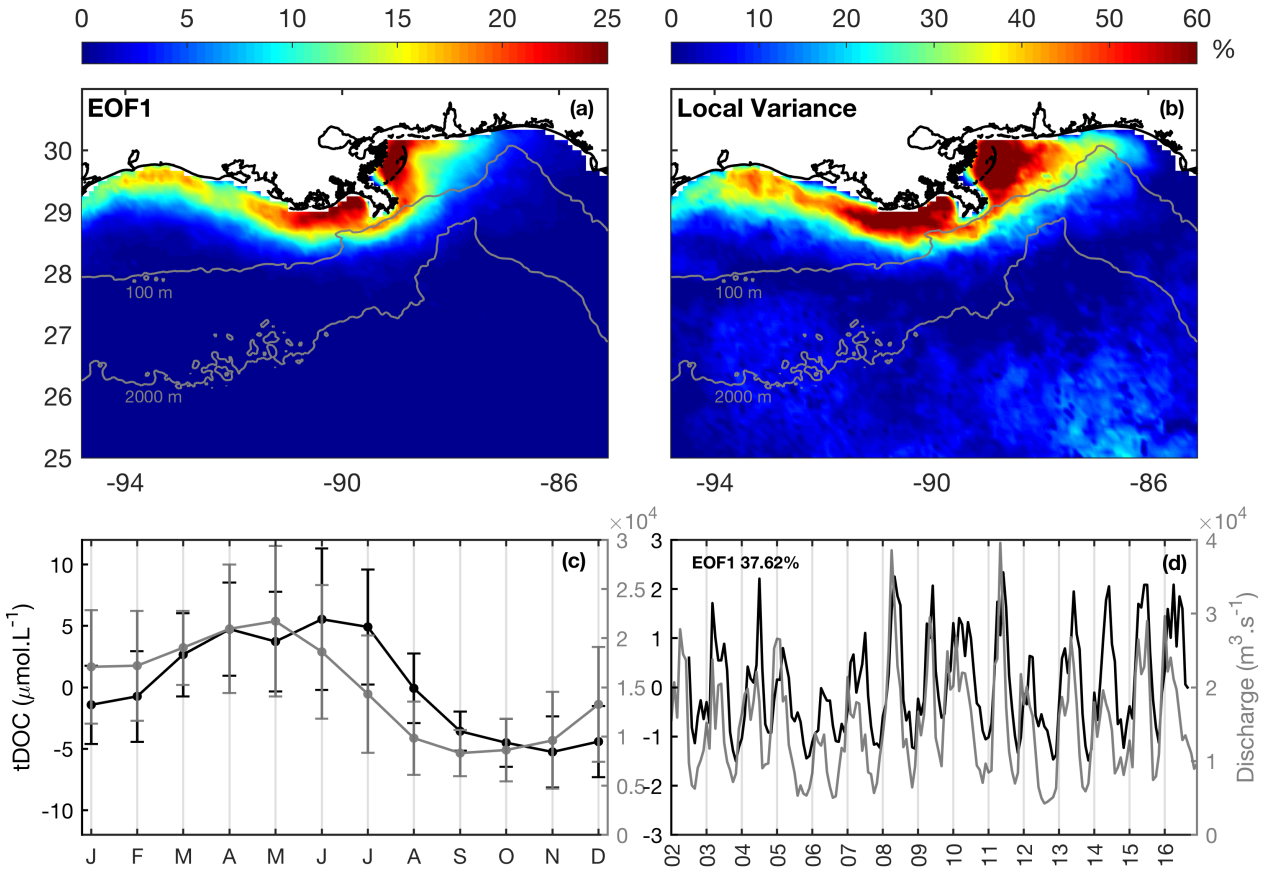

Figure 2.5. (a) First EOF of tDOC concentration. (b) Fraction of the local variance explained by the first EOF mode (c) Monthly average of the amplitude time series of EOF 1 (black) and of the Mississippi River discharge (gray). (d) Amplitude time series of EOF 1 (black) and MR discharge (gray).

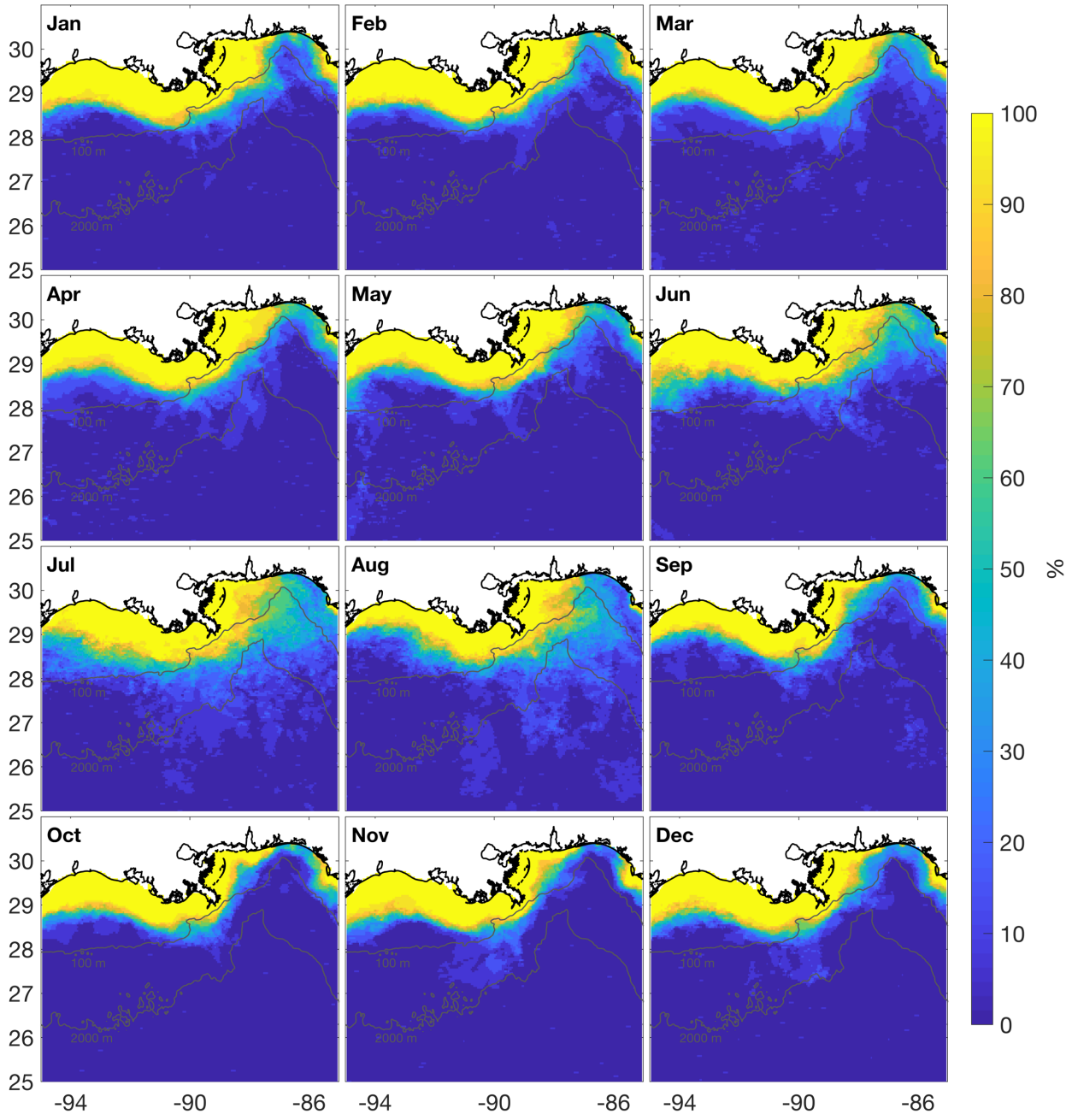

Figure 2.6. Mean monthly frequency of plume occurrence in the northern Gulf of Mexico. The gray lines represent the 100 and 2000 m isobaths.

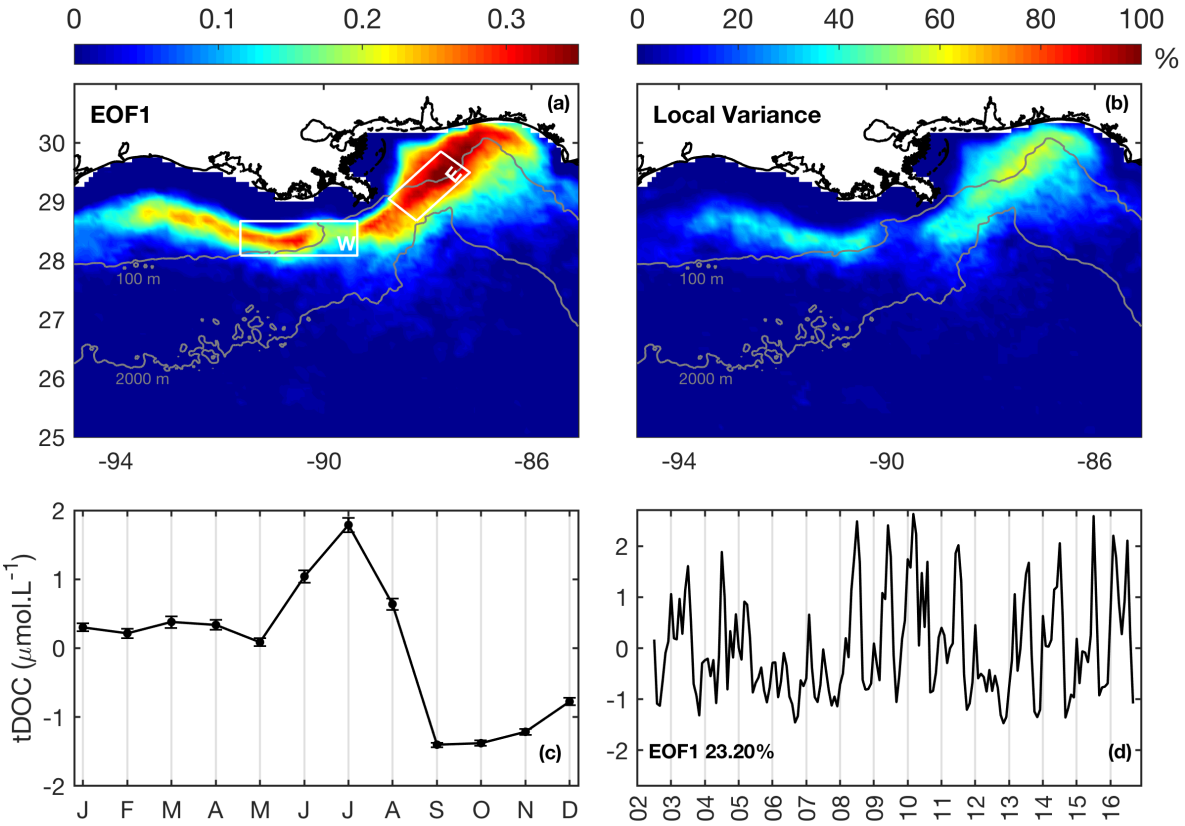

Figure 2.7. (a) First EOF of frequency of plume occurrence. White boxes show locations where average alongshore winds were computed, Box West (W) and Box East (E). (b) Fraction of the local variance explained by the first EOF mode (c) Monthly average of the amplitude time series of EOF 1. (d) Amplitude time series of EOF 1.

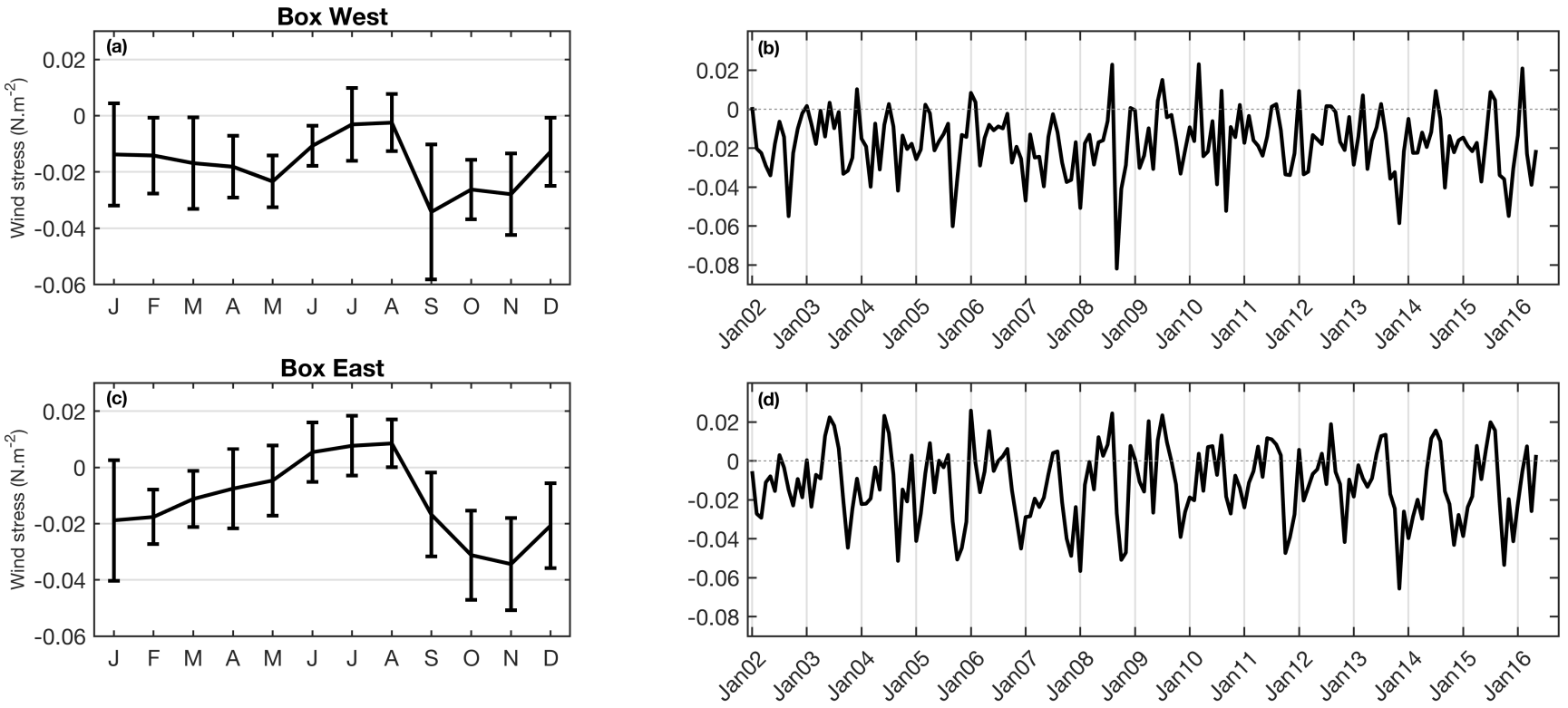

Figure 2.8. Alongshore wind stress at Boxes West and East (see Figure 2.7a for location). Upwelling favorable winds are positive. Monthly averages are shown on left panels (a and c), while the time series for the entire period are shown on the right (b and d).

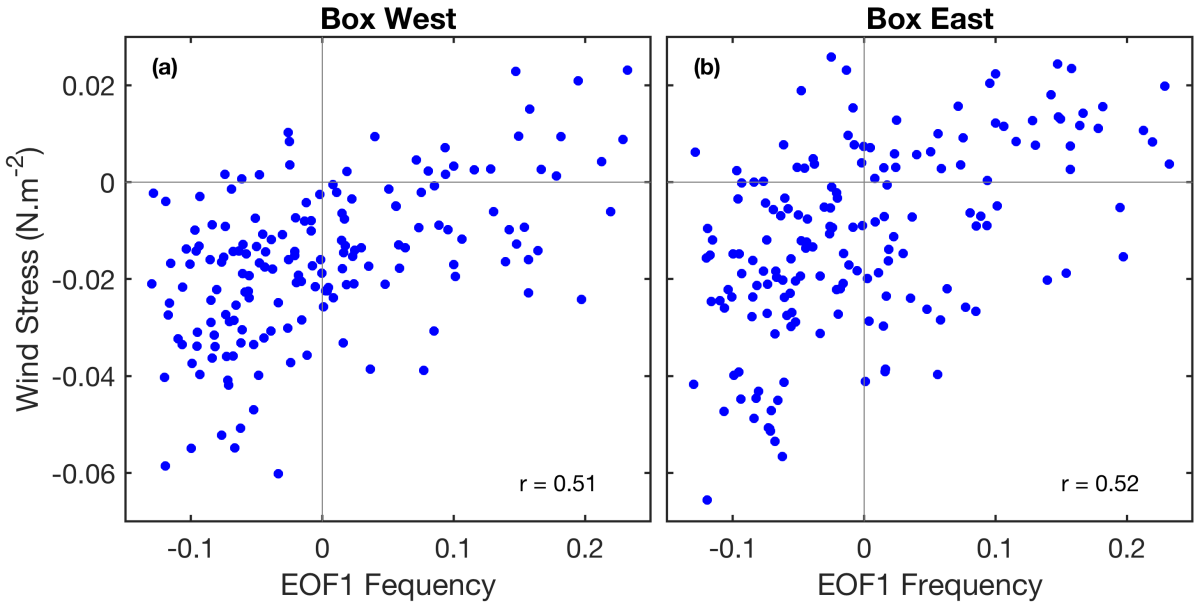

Figure 2.9. Relation between alongshore wind stress at Boxes (a) West and (b) East (from Figure 2.8; upwelling favorable winds are positive) and the amplitude time series of EOF 1 of the frequency of plume occurrence (from Figure 2.7d).

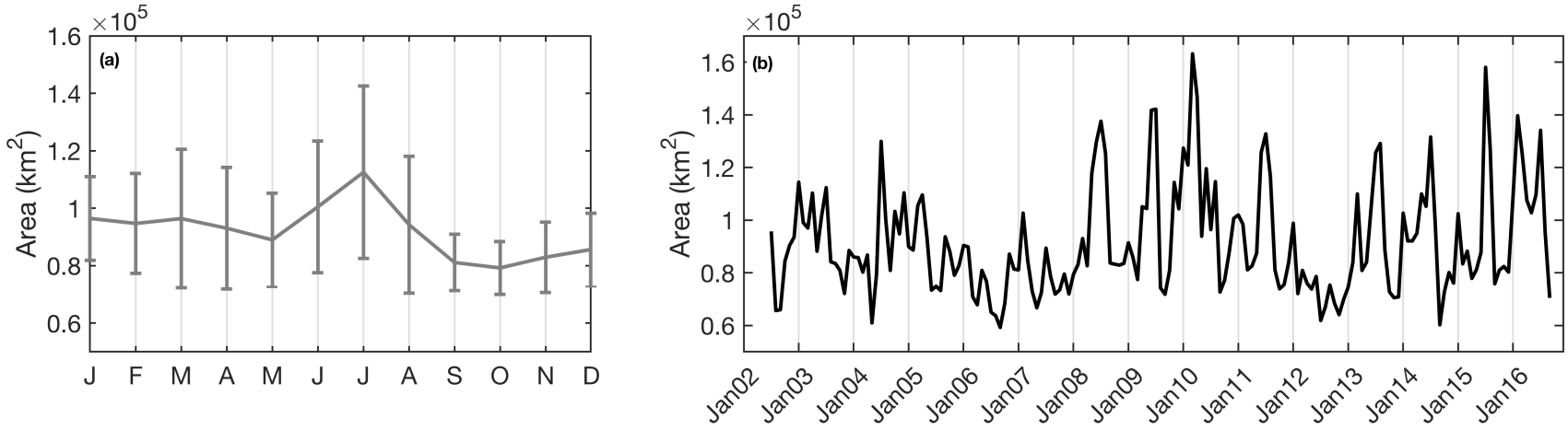

Figure 2.10. MR plume area (km^2) as identified by applying a boundary-detection algorithm to MODIS tDOC data. (a) Monthly averaged data and (b) monthly time series.

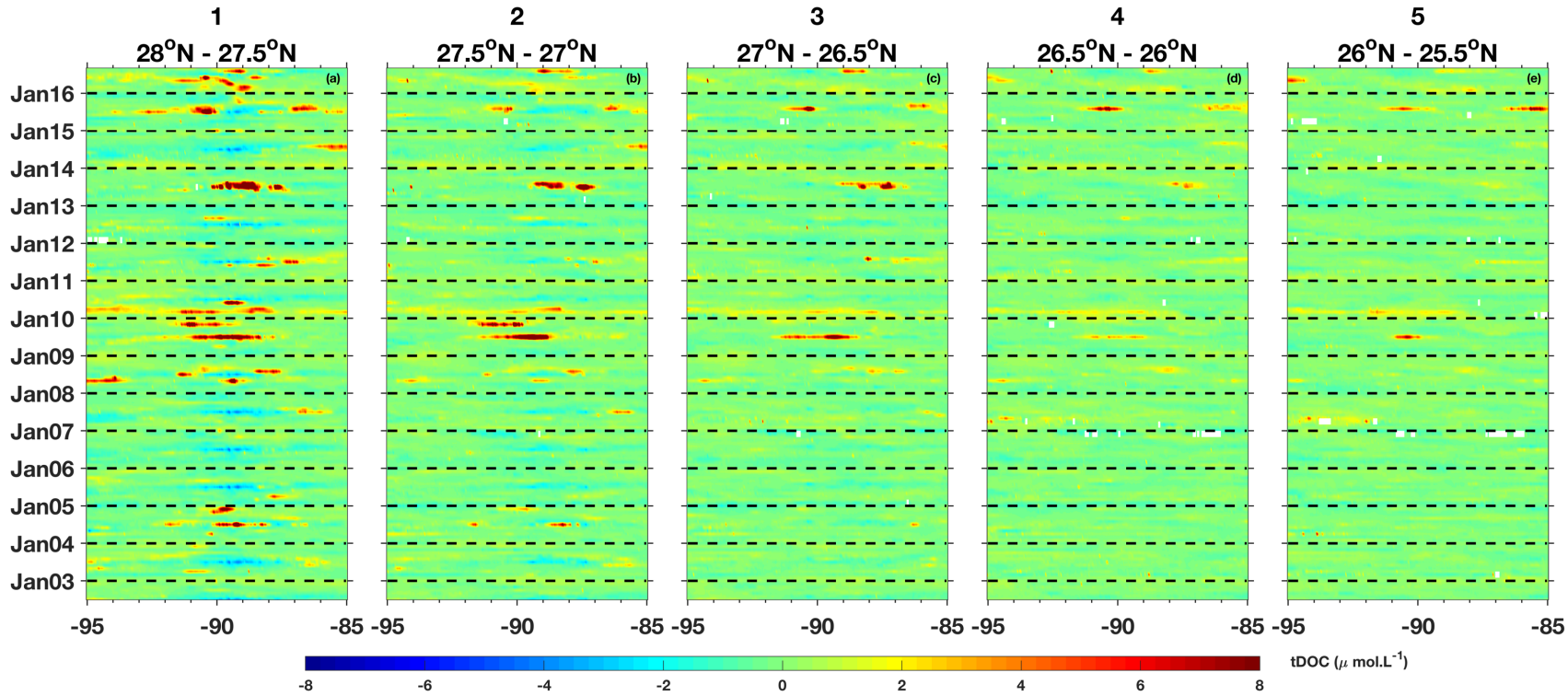

Figure 2.11. Hovmöller diagrams of tDOC anomaly concentration along 5 (a-e) bands in the northern Gulf of Mexico. Location of zonal bands in shown in Figure 2.4. Anomaly is defined as the deviation from the seasonal cycle.

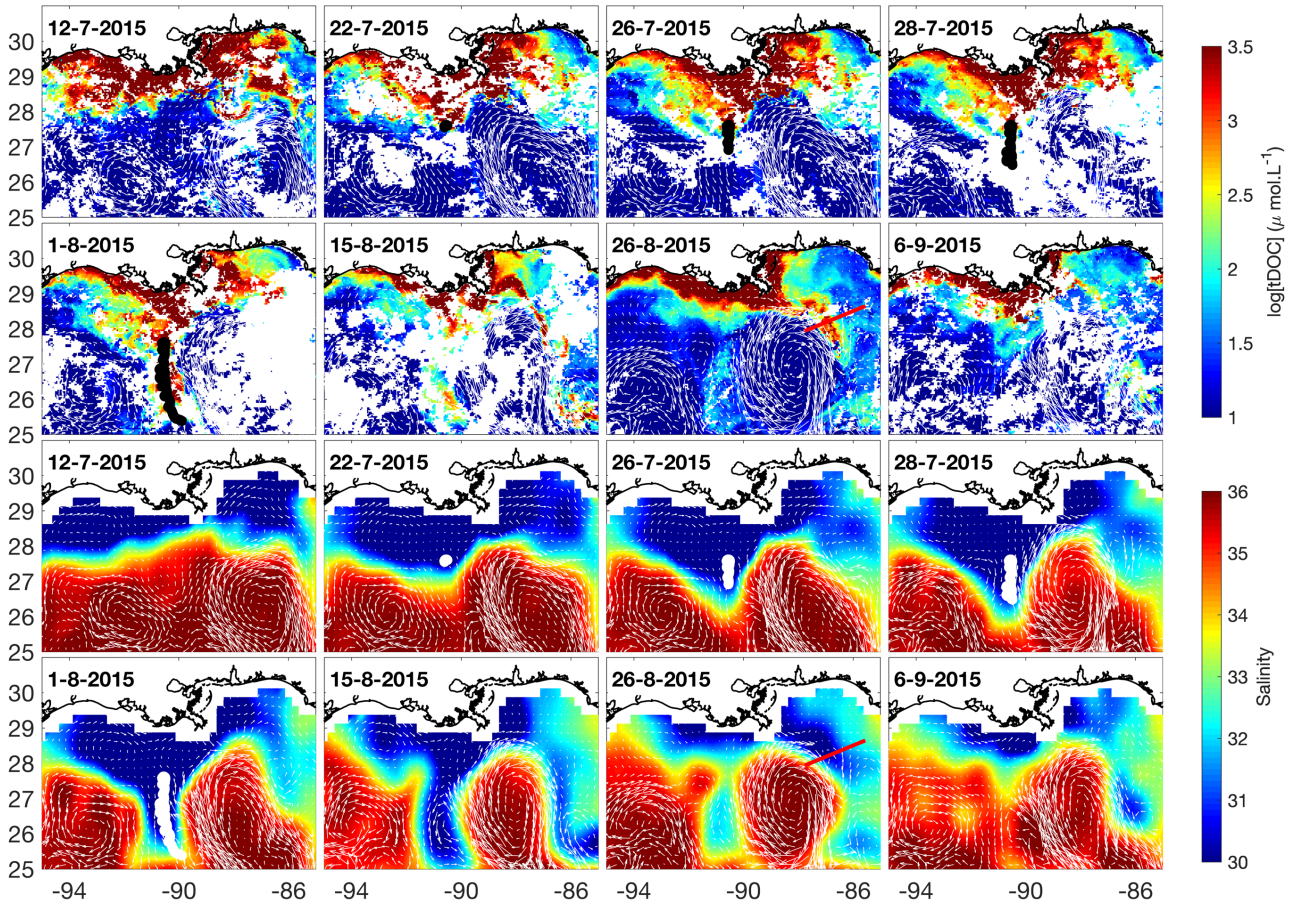

Figure 2.12. Extreme event of offshore transport of MRP in 2015 based on MODIS tDOC and SMAP SSS. The black and white dots show track of surface drifter. Arrows show geostrophic velocity from altimetry. Transect used to compare tDOC and SSS data (in Figure 2.14) is shown in red. Data from all days from 11 July to 8 September are shown in Appendix A Figures A2 and A3.

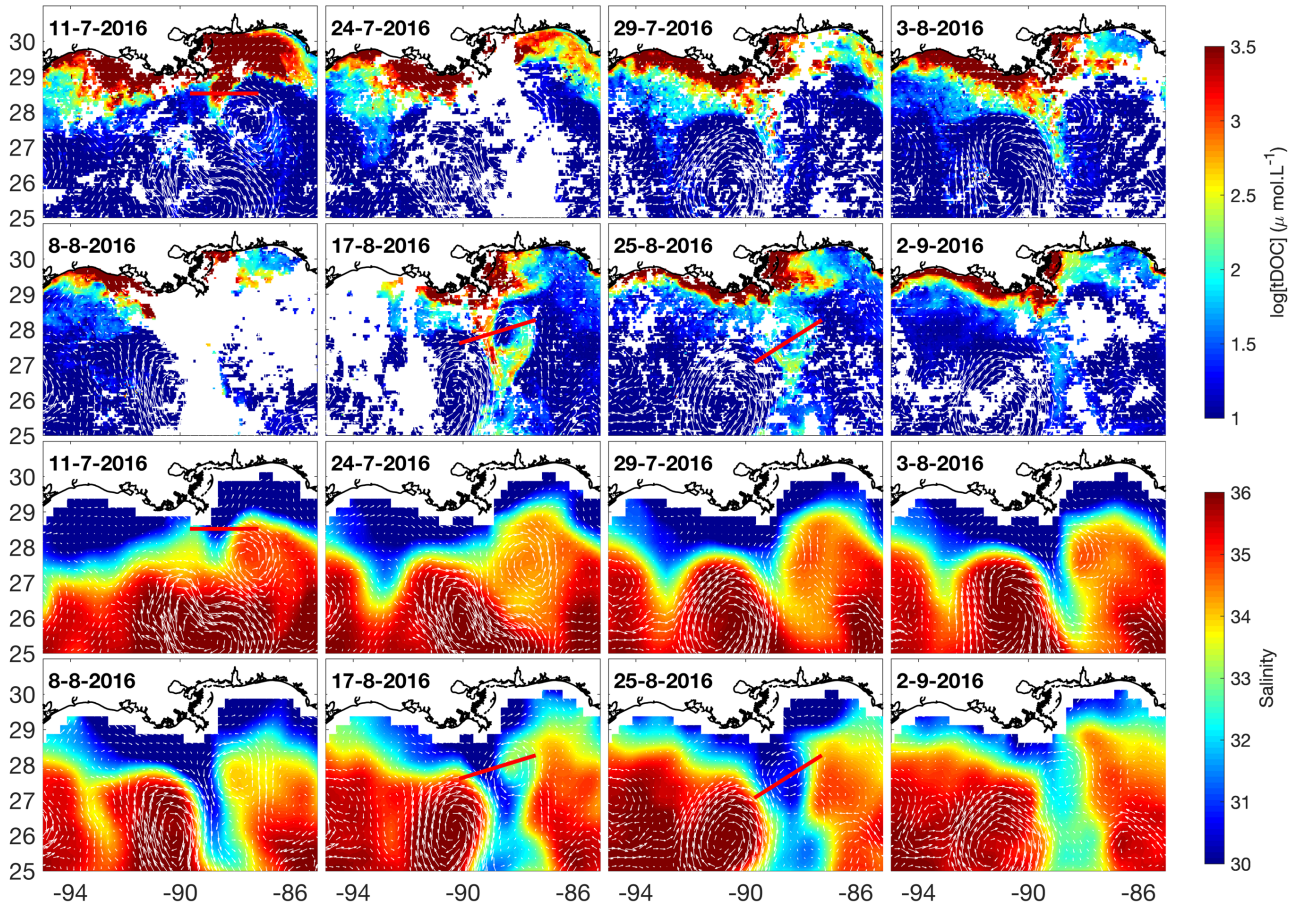

Figure 2.13. Extreme event of offshore transport of MRP in 2016 based on MODIS tDOC and SMAP SSS. Arrows show geostrophic velocity from altimetry. Transects used to compare tDOC and SSS data (in Figure 2.14) are shown in red. Data from all days from 11 July to 2 September are shown in Appendix A Figures A4 and A5.

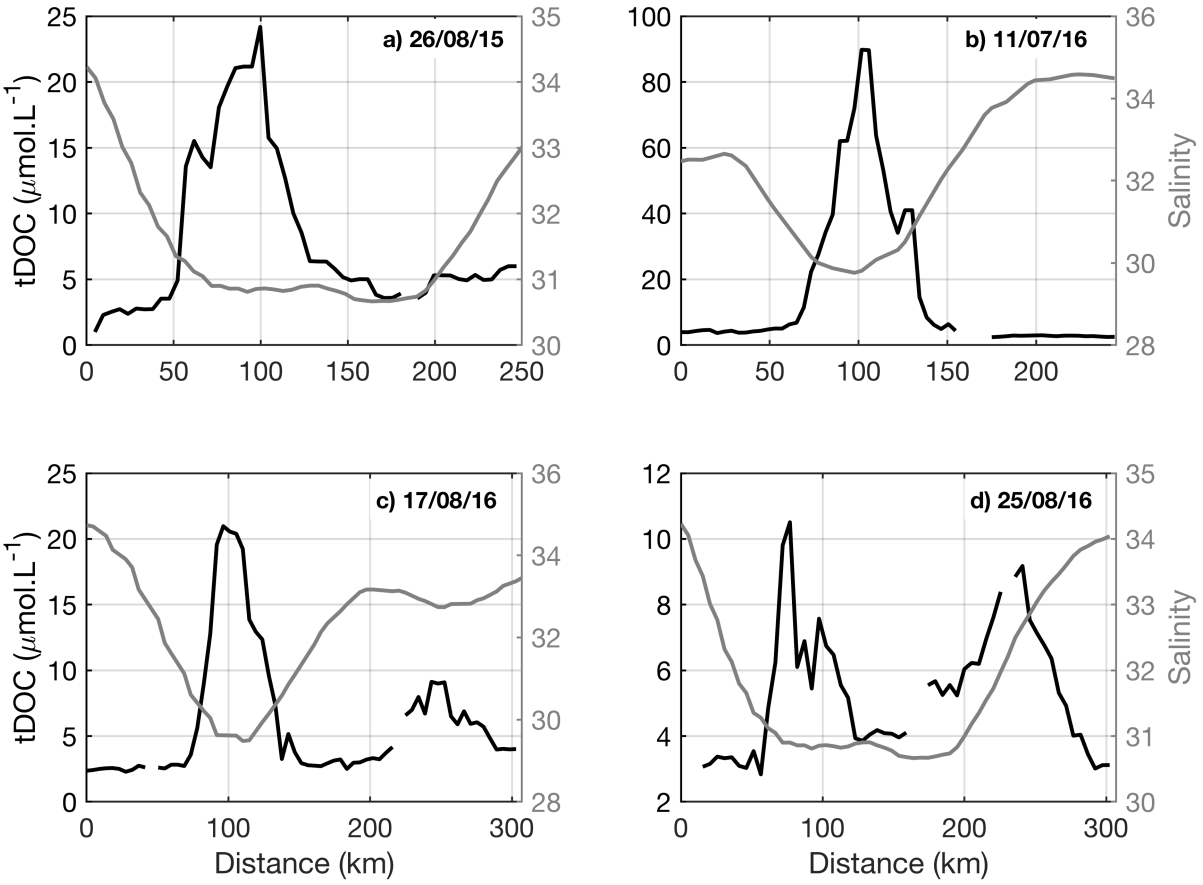

Figure 2.14. Comparison between SMAP SSS and MODIS tDOC along transects shown in Figures 2.12 and 2.13.

CHAPTER 3

SUMMARY AND FURTHER STEPS

3.1. Summary

The Mississippi River has a great influence in coastal processes in the Gulf of Mexico due to the amount of freshwater and other terrigenous material that it delivers to the ocean. After the 2010 Oil Spill, the Mississippi River plume and Gulf of Mexico circulation received a great attention from the oceanographic community. Understanding the fate of the riverine waters and how they interact with the Gulf of Mexico circulation became crucial to improve predictions of oil dispersion in the ocean.

A general description of the river plumes and the main mechanisms that can influence their dynamics was presented in chapter 1. Although much has been learned about the Mississippi River plume dynamics over the last decade or so, many of the previous studies were constrained by the low temporal and spatial resolution of the data sets used (e.g. moorings, cruises profiles). Most previous studies were also focused in the coastal regions over the shelf in the northern Gulf of Mexico. The recent advance of new satellite data products spanning long periods with improved spatial resolution allows us to investigate plume distribution and variability in much greater detail. Describing MRP variability is the main focus of chapter 2, where it was shown that the MRP extends offshore during the summer when winds tend to be more upwelling-favorable. A new contribution of this research was the mapping of the regions of the Gulf of Mexico

influenced by riverine-waters and quantifying the frequency of plume occurrence. This has important biogeochemical implications, since riverine influenced waters are an important source of nutrients to the region. The analysis reveals that the river plume distribution on monthly time scales is driven primarily by river discharge and by winds. On shorter time scales of a few days, however, the MRP offshore transport is driven by the interactions with the Loop Current and associated eddies, which is facilitated by the steep topography of the Gulf of Mexico in the delta vicinity.

The new satellite data sets used allowed for a more complete description of the MRP distribution and variability. This is especially true when SMAP SSS and MODIS tDOC are using in combination, since each data set independently presents important limitations. While tDOC data are influenced by clouds and only provide an indirect representation of the river plume, the high resolution of the observations allow for a more accurate representation of sharp fronts and narrow filaments of coastal water being transported offshore. Cloud coverage can severely limit data availability during specific periods, however, such as during the 2015 and 2016 events described in chapter 2. On the other hand, despite the relatively large SMAP footprint (~ 40 km), the satellite is not affected by clouds and provided a good view of the daily evolution of these events. This research demonstrated that the combined usage of SMAP SSS and MODIS-Aqua tDOC is an improved approach to investigate riverine-influenced regions.

3.2. Further Steps: Formation of Mississippi River Plume Filaments by Mesoscale Eddies

In the previous chapter, the importance of eddies in transporting the Mississippi River Plume offshore was shown based on MODIS-Aqua tDOC and SMAP SSS measurements. Because the river plume is simultaneously influenced by a variety of forcing, it is often difficult to isolate the influence of eddies based on observations alone. As such, idealized modeling simulations can provide useful information about the formation of Mississippi River Plume filaments due to interactions with mesoscale eddies.

Eddies are important features in the ocean. They have been shown to play an important role on the transport of heat (De Ruijter et al., 1999; Wunsch 1999; Roemmich and Gilson 2001; Crawford, 2005), salt (Ballegooyen et al., 1994; Treguier et al., 2012; Dong et al., 2014), and biogeochemical properties (Garcon et al., 2001; Chelton et al., 2011a) to different places in the ocean. Also, they can promote large-scale mixing in the ocean (Abernathey et al., 2009) and interact with the mean flow (Olbers 2005). Eddies are generally referred to as warm- or cold-core, depending of the temperature anomaly in their interior. While cyclonic eddies are characterized by cold anomalies in their interior (cold-core eddies), anticyclonic eddies are characterized by warm anomalies. Eddies can be found nearly everywhere in the ocean (Chelton et al., 2011a). However, the most energetic are in general associated with western boundary currents (e.g.; Gulf Stream, Agulhas Current; Chelton et al., 2011b). This is because a meandering western boundary current creates unstable regions which are often favorable for eddy formation. These

mesoscale eddies generally have a radius of 50-100 kilometers and can persist for periods of many months.

Cenedese et al. (2013) showed based on laboratory experiments that the interaction of anticyclonic vortices with a coastally trapped buoyant plume can result in the generation of coastal filaments that are transported towards the open ocean. This occurs when the ratio ($\in$) between the azimuthal velocity in the eddy and maximum along shelf velocity in the shelfbreak is greater than 1. When the ratio is smaller than 1 filament formation can still occur, but it reconnects with the shelfbreak current resulting in no net offshore transport. In the same study, the authors simulated the interaction between cyclonic eddies and the shelfbreak current. In contrast to anticyclones, they found that cyclonic eddies tend to "squeeze" the shelf current close to the coast. As such, no significant offshore transport of coastal water was observed. Zhang and Gawarkiewicz (2015) also demonstrated that cyclonic eddies from the Gulf Stream can intrude onto the shelfbreak with important biogeochemical implications.

The analyses of MODIS tDOC data and of geostrophic velocities from altimetry indicate that the interaction of cyclonic eddies with the Mississippi River plume can sometimes result in the offshore transport of river-influenced waters (Figure 3.1), which is in contrast with Cenedese et al. (2013) laboratory experiments. A possible explanation for this discrepancy is that Cenedese et al. (2013) did not consider wind forcing in their experiments. One hypothesis is that significant filaments due to cyclones will only be formed if currents at the boundary of the buoyant plume oppose the azimuthal velocity around the cyclonic eddy (e.g., if winds, which were not considered in Cenedese et al.'s (2013) experiments, are upwelling favorable and strong enough to reverse the flow near

the front; note that winds during summer generally promote eastward transport of riverine waters in the region, Morey et al., 2003). This hypothesis can be tested using model simulations. Specifically, idealized model simulations should include the interaction of an anticyclonic eddy or of a cyclonic eddy with a river plume under the influence of wind forcing from different directions and magnitudes, from strongly downwelling favorable to strongly upwelling favorable. These simulations would allow for identifying the conditions in which filaments can be formed due to the interactions of cyclones with the river plume. They would additionally allow for testing the hypothesis that these filaments can only be formed if winds are upwelling favorable and strong enough to reverse the current direction near the offshore boundary of the plume. Testing this hypothesis awaits future studies.

Figures

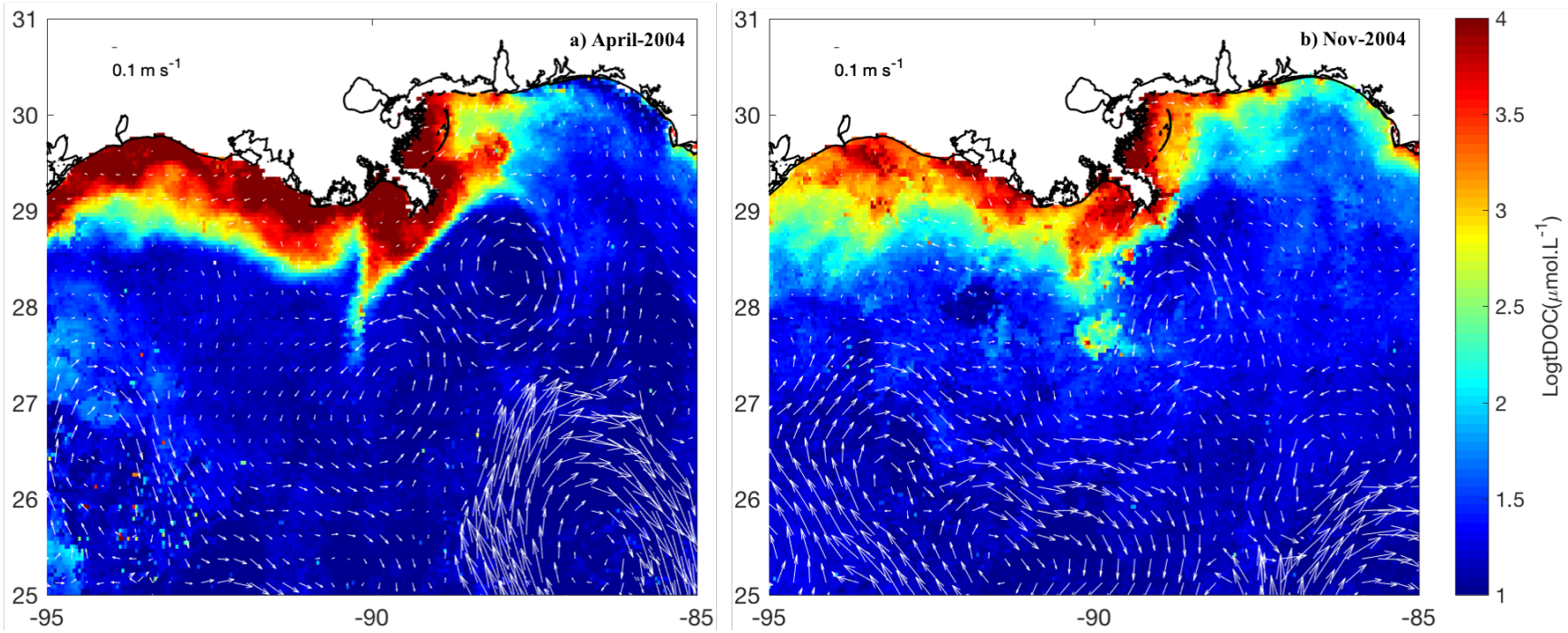

Figure 3.1. Filaments formed by cyclonic eddies in April 2004 (a) and November 2004 (b).

REFERENCES

Abernathey, R., Marshall, J., Mazloff, M., & Shuckburgh, E. (2010). Enhancement of mesoscale eddy stirring at steering levels in the Southern Ocean. *Journal of Physical Oceanography*, *40*(1), 170-184. *https://doi.org/10.1175/2009JPO4201.1*

Androulidakis, Y. S., & Kourafalou, V. H. (2013). On the processes that influence the transport and fate of Mississippi waters under flooding outflow conditions. *Ocean Dynamics*, *63*(2-3), 143-164. https://doi.org/10.1109/5.771073

Atlas, R., Hoffman, R. N., Ardizzone, J., Leidner, S. M., Jusem, J. C., Smith, D. K., & Gombos, D. (2011). A cross-calibrated, multiplatform ocean surface wind velocity product for meteorological and oceanographic applications. *Bulletin of the American Meteorological Society*, *92*(2), 157-174. https://doi.org/10.1109/IGARSS.2008.4778804

Ballegooyen, R. C., Gründlingh, M. L., & Lutjeharms, J. R. (1994). Eddy fluxes of heat and salt from the southwest Indian Ocean into the southeast Atlantic Ocean: A case study. *Journal of Geophysical Research: Oceans*, *99*(C7), 14053-14070. https://doi.org/10.1029/94JC00383

Belkin, I. M., & O'Reilly, J. E. (2009). An algorithm for oceanic front detection in chlorophyll and SST satellite imagery. *Journal of Marine Systems*, *78*(3), 319-326. https://doi.org/10.1016/j.jmarsys.2008.11.018

Benner, R., & Opsahl, S. (2001). Molecular indicators of the sources and transformations of dissolved organic matter in the Mississippi river plume. *Organic Geochemistry*, *32*(4), 597-611. https://doi.org/10.1016/S0146-6380(00)00197-2

Bianchi, T. S., DiMarco, S. F., Cowan Jr, J. H., Hetland, R. D., Chapman, P., Day, J. W., & Allison, M. A. (2010). The science of hypoxia in the Northern Gulf of Mexico: a review. *Science of the Total Environment*, *408*(7), 1471-1484. https://doi.org/10.1016/j.scitotenv.2009.11.047

Boutin, J., Chao, Y., Asher, W. E., Delcroix, T., Drucker, R., Drushka, K., ... & Schanze, J. (2016). Satellite and *in situ* salinity: Understanding near-surface stratification and subfootprint variability. *Bulletin of the American Meteorological Society*, *97*(8), 1391-1407. https://doi.org/10.1175/BAMS-D-15-00032.1

Canny, J. (1987). A computational approach to edge detection. In *Readings in Computer Vision* (pp. 184-203). https://doi.org/10.1016/B978-0-08-051581-6.50024-6

Castelao, R. M., Mavor, T. P., Barth, J. A., & Breaker, L. C. (2006). Sea surface temperature fronts in the California Current System from geostationary satellite observations. *Journal of Geophysical Research: Oceans*, *111*(C9). https://doi.org/10.1029/2006JC003541

Castelao, R., Schofield, O., Glenn, S., Chant, R., & Kohut, J. (2008). Cross-shelf transport of freshwater on the New Jersey shelf. *Journal of Geophysical Research: Oceans*, *113*(C7). https://doi.org/10.1029/2007JC004241

Cayula, J. F., & Cornillon, P. (1992). Edge detection algorithm for SST images. *Journal of Atmospheric and Oceanic Technology*, *9*(1), 67-80. https://doi.org/10.1175/1520-0426(1992)009%3C0067:EDAFSI%3E2.0.CO;2

Cenedese, C., Todd, R. E., Gawarkiewicz, G. G., Owens, W. B., & Shcherbina, A. Y. (2013). Offshore transport of shelf waters through interaction of vortices with a shelfbreak current. *Journal of Physical Oceanography*, *43*(5), 905-919. *https://doi.org/10.1175/JPO-D-12-0150.1*

Chao, Y., Farrara, J. D., Schumann, G., Andreadis, K. M., & Moller, D. (2015). Sea surface salinity variability in response to the Congo River discharge. *Continental Shelf Research*, *99*, 35-45. https://doi.org/10.1016/j.csr.2015.03.005

Chelton, D. B., Gaube, P., Schlax, M. G., Early, J. J., & Samelson, R. M. (2011b). The influence of nonlinear mesoscale eddies on near-surface oceanic chlorophyll. *Science*, *334*(6054), 328-332.https://doi.org/10.1126/science.1208897

Chelton, D. B., Schlax, M. G., & Samelson, R. M. (2011a). Global observations of nonlinear mesoscale eddies. *Progress in Oceanography*, *91*(2), 167-216. https://doi.org/10.1016/j.pocean.2011.01.002

Chesney, E. J., Baltz, D. M., & Thomas, R. G. (2000). Louisiana estuarine and coastal fisheries and habitats: perspectives from a fish's eye view. *Ecological Applications*, *10*(2), 350-366. https://doi.org/10.1890/1051-0761(2000)010[0350:LEACFA]2.0.CO;2

Choi, B. J., & Wilkin, J. L. (2007). The effect of wind on the dispersal of the Hudson River plume. Journal of Physical Oceanography, 37(7), 1878-1897.

Cochrane, J. D., & Kelly, F. J. (1986). Low-frequency circulation on the Texas-Louisiana continental shelf. *Journal of Geophysical Research: Oceans*, *91*(C9), 10645-10659. https://doi.org/10.1029/JC091iC09p10645

Crawford, W. R. (2005). Heat and fresh water transport by eddies into the Gulf of Alaska. *Deep Sea Research Part II: Topical Studies in Oceanography*, *52*(7-8), 893-908. https://doi.org/10.1016/j.dsr2.2005.02.003

Davis, R. E. (1985). Drifter observations of coastal surface currents during CODE: The statistical and dynamical views. *Journal of Geophysical Research: Oceans*, *90*(C3), 4756-4772. https://doi.org/10.1029/JC090iC03p04756

Degens, E. T., Kempe, S., & Richey, J. E. (1991). SCOPE 42: Biogeochemistry of major world rivers. *UK: Wiley*.

Del Castillo, C. E., Coble, P. G., Conmy, R. N., Müller-Karger, F. E., Vanderbloemen, L., & Vargo, G. A. (2001). Multispectral *in situ* measurements of organic matter and chlorophyll fluorescence in seawater: documenting the intrusion of the Mississippi River plume in the West Florida Shelf. *Limnology and Oceanography*, *46*(7), 1836-1843. https://doi.org/10.4319/lo.2001.46.7.1836

Dinnel, S. P., & Wiseman Jr, W. J. (1986). Fresh water on the Louisiana and Texas shelf. *Continental Shelf Research*, *6*(6), 765-784. https://doi.org/10.1016/0278-4343(86)90036-1

Dohan, K., Kao, H. Y., & Lagerloef, G. S. (2015). The Freshwater Balance: Over the North Atlantic SPURS Domain from Aquarius Satellite Salinity, OSCAR Satellite Surface Currents, and Some Simplified Approaches. *Oceanography*, *28*(1), 86-95.

Dong, C., McWilliams, J. C., Liu, Y., & Chen, D. (2014). Global heat and salt transports by eddy movement. *Nature communications*, *5*, 3294. https://doi.org/10.1038/ncomms4294

Durack, P. J., Lee, T., Vinogradova, N. T., & Stammer, D. (2016). Keeping the lights on for global ocean salinity observation. *Nature Climate Change*, *6*(3), 228. https://doi.org/10.1038/nclimate2946

Entekhabi, D., Njoku, E. G., O'Neill, P. E., Kellogg, K. H., Crow, W. T., Edelstein, W. N., ... & Kimball, J. (2010). The soil moisture active passive (SMAP) mission. *Proceedings of the IEEE*, *98*(5), 704-716. https://doi.org/10.1109/JPROC.2010.2043918

Fichot, C. G., & Benner, R. (2012). The spectral slope coefficient of chromophoric dissolved organic matter (S275–295) as a tracer of terrigenous dissolved organic carbon in river-influenced ocean margins. *Limnology and Oceanography*, *57*(5), 1453-1466. https://doi.org/10.4319/lo.2012.57.5.1453

Fichot, C. G., Kaiser, K., Hooker, S. B., Amon, R. M., Babin, M., Bélanger, S., ... & Benner, R. (2013). Pan-Arctic distributions of continental runoff in the Arctic Ocean. *Scientific reports*, *3*, 1053. https://doi.org/10.1038/srep01053

Fichot, C. G., Lohrenz, S. E., & Benner, R. (2014). Pulsed, cross-shelf export of terrigenous dissolved organic carbon to the Gulf of Mexico. *Journal of Geophysical Research: Oceans*, *119*(2), 1176-1194. https://doi.org/10.1002/2013JC009424

Fong, D. A., & Geyer, W. R. (2001). Response of a river plume during an upwelling favorable wind event. *Journal of Geophysical Research: Oceans*, *106*(C1), 1067-1084. https://doi.org/10.1029/2000JC900134

Fong, D. A., Geyer, W. R., & Signell, R. P. (1997). The wind-forced response on a buoyant coastal current: Observations of the western Gulf of Maine plume. Journal of Marine Systems, 12(1-4), 69-81.

Fore, A. G., Yueh, S. H., Tang, W., Stiles, B. W., & Hayashi, A. K. (2016). Combined active/passive retrievals of ocean vector wind and sea surface salinity with SMAP. *IEEE Transactions on Geoscience and Remote Sensing*, *54*(12), 7396-7404. https://doi.org/10.1109/TGRS.2016.2601486

Fournier, S., Chapron, B., Salisbury, J., Vandemark, D., & Reul, N. (2015). Comparison of spaceborne measurements of sea surface salinity and colored detrital matter in the Amazon plume. *Journal of Geophysical Research: Oceans*, *120*(5), 3177-3192. https://doi.org/10.1002/2014JC010109

Fournier, S., Lee, T., & Gierach, M. M. (2016). Seasonal and interannual variations of sea surface salinity associated with the Mississippi River plume observed by SMOS and Aquarius. *Remote sensing of environment*, *180*, 431-439. https://doi.org/10.1016/j.rse.2016.02.050

Fournier, S., Vialard, J., Lengaigne, M., Lee, T., Gierach, M. M., & Chaitanya, A. V. S. (2017). Modulation of the Ganges-Brahmaputra River Plume by the Indian Ocean Dipole and Eddies Inferred from Satellite Observations. *Journal of Geophysical Research: Oceans*, *122*(12), 9591-9604. https://doi.org/10.1002/2017JC013333

Garçon, V. C., Oschlies, A., Doney, S. C., McGillicuddy, D., & Waniek, J. (2001). The role of mesoscale variability on plankton dynamics in the North Atlantic. *Deep Sea Research Part II: Topical Studies in Oceanography*, *48*(10), 2199-2226. https://doi.org/10.1016/S0967-0645(00)00183-1

Gierach, M. M., Vazquez-Cuervo, J., Lee, T., & Tsontos, V. M. (2013). Aquarius and SMOS detect effects of an extreme Mississippi River flooding event in the Gulf of

Mexico. *Geophysical Research Letters*, *40*(19), 5188-5193. https://doi.org/10.1002/grl.50995

Gilbert, P. S., Lee, T. N., & Podesta, G. P. (1996). Transport of anomalous low-salinity waters from the Mississippi River flood of 1993 to the Straits of Florida. *Continental Shelf Research*, *16*(8), 1065-1085. https://doi.org/10.1016/0278-4343(95)00056-9

Green, R. E., Bianchi, T. S., Dagg, M. J., Walker, N. D., & Breed, G. A. (2006). An organic carbon budget for the Mississippi River turbidity plume and plume contributions to air-sea CO 2 fluxes and bottom water hypoxia. *Estuaries and Coasts*, *29*(4), 579-597. https://doi.org/10.1007/BF02784284

Grodsky, S. A., Reul, N., Lagerloef, G., Reverdin, G., Carton, J. A., Chapron, B., ... & Kao, H. Y. (2012). Haline hurricane wake in the Amazon/Orinoco plume: AQUARIUS/SACD and SMOS observations. *Geophysical Research Letters*, *39*(20). https://doi.org/10.1029/2012GL053335

Grodsky, S. A., Reverdin, G., Carton, J. A., & Coles, V. J. (2014). Year-to-year salinity changes in the Amazon plume: Contrasting 2011 and 2012 Aquarius/SACD and SMOS satellite data. *Remote sensing of environment*, *140*, 14-22. https://doi.org/10.1016/j.rse.2013.08.033

Hedges, J. I., & Parker, P. L. (1976). Land-derived organic matter in surface sediments from the Gulf of Mexico. *Geochimica et Cosmochimica Acta*, *40*(9), 1019-1029. https://doi.org/10.1016/0016-7037(76)90044-2

Helms, J. R., Stubbins, A., Ritchie, J. D., Minor, E. C., Kieber, D. J., & Mopper, K. (2008). Absorption spectral slopes and slope ratios as indicators of molecular weight, source,

and photobleaching of chromophoric dissolved organic matter. *Limnology and Oceanography*, *53*(3), 955-969. https://doi.org/10.4319/lo.2008.53.3.0955

Hu, C., Nelson, J. R., Johns, E., Chen, Z., Weisberg, R. H., & Müller-Karger, F. E. (2005). Mississippi River water in the Florida Straits and in the Gulf Stream off Georgia in summer 2004. *Geophysical Research Letters*, *32*(14). https://doi.org/10.1029/2005GL022942

Huang, W. J., Cai, W. J., Castelao, R. M., Wang, Y., & Lohrenz, S. E. (2013). Effects of a wind-driven cross-shelf large river plume on biological production and CO2 uptake on the Gulf of Mexico during spring. *Limnology and Oceanography*, *58*(5), 1727-1735. https://doi.org/10.4319/lo.2013.58.5.1727

Huh, O. K., Wiseman, W. J., & Rouse, L. J. (1981). Intrusion of Loop Current waters onto the west Florida continental shelf. Journal of Geophysical Research: Oceans, 86(C5), 4186-4192.

Jurisa, J. T., & Chant, R. J. (2013). Impact of offshore winds on a buoyant river plume system. *Journal of Physical Oceanography*, *43*(12), 2571-2587. https://doi.org/10.1175/JPO-D-12-0118.1

Kostianoy, A. G., Ginzburg, A. I., Frankignoulle, M., & Delille, B. (2004). Fronts in the Southern Indian Ocean as inferred from satellite sea surface temperature data. *Journal of Marine Systems*, *45*(1-2), 55-73. https://doi.org/10.1016/j.jmarsys.2003.09.004

Lagerloef, G. E., Colomb, R., Le Vine, D., Wetz, F., Yueh, S., Ruf, C., ... & Feldman, G. (2008). The Aquarius/SAC-D mission: special issue on salinity. *Oceanography*, *21*(1), 69-81. http://www.jstor.org/stable/24860158

Lentz, S. (2004). The response of buoyant coastal plumes to upwelling-favorable winds. *Journal of Physical oceanography*, *34*(11), 2458-2469. https://doi.org/10.1175/JPO2647.1

Lohrenz, S. E., Dagg, M. J., & Whitledge, T. E. (1990). Enhanced primary production at the plume/oceanic interface of the Mississippi River. *Continental shelf research*, *10*(7), 639-664. https://doi.org/10.1016/0278-4343(90)90043-L

Luo, H., Bracco, A., Cardona, Y., & McWilliams, J. C. (2016). Submesoscale circulation in the northern Gulf of Mexico: Surface processes and the impact of the freshwater river input. *Ocean Modelling*, *101*, 68-82. https://doi.org/10.1016/j.ocemod.2016.03.003

Mavor, T. P., & Bisagni, J. J. (2001). Seasonal variability of sea-surface temperature fronts on Georges Bank. *Deep Sea Research Part II: Topical Studies in Oceanography*, *48*(1-3), 215-243. https://doi.org/10.1016/S0967-0645(00)00120-X

Medeiros, P. M., Babcock-Adams, L., Seidel, M., Castelao, R. M., Di Iorio, D., Hollibaugh, J. T., & Dittmar, T. (2017). Export of terrigenous dissolved organic matter in a broad continental shelf. *Limnology and Oceanography*, *62*(4), 1718-1731. https://doi.org/10.1002/lno.10528

Meissner, T., & Wentz, F. (2016). Remote sensing systems SMAP L3 monthly sea surface salinity on 0.25 deg grid Version 2.0 validated release. *Remote Sens. Syst., Santa Rosa, CA, USA, Tech. Rep*.

Miller, P. (2004). Multi-spectral front maps for automatic detection of ocean colour features from SeaWiFS. *International Journal of Remote Sensing*, *25*(7-8), 1437-1442. https://doi.org/10.1080/01431160310001592409

Milliman, J. D., & Meade, R. H. (1983). World-wide delivery of river sediment to the oceans. *The Journal of Geology*, *91*(1), 1-21. https://doi.org/10.1086/628741

Molleri, G. S., Novo, E. M. D. M., & Kampel, M. (2010). Space-time variability of the Amazon River plume based on satellite ocean color. *Continental Shelf Research*, *30*(3-4), 342-352. https://doi.org/10.1016/j.csr.2009.11.015

Moore, J. K., Abbott, M. R., & Richman, J. G. (1997). Variability in the location of the Antarctic Polar Front (90–20 W) from satellite sea surface temperature data. *Journal of Geophysical Research: Oceans*, *102*(C13), 27825-27833. https://doi.org/10.1029/97JC01705

Morey, S. L., Martin, P. J., O'Brien, J. J., Wallcraft, A. A., & Zavala-Hidalgo, J. (2003b). Export pathways for river discharged fresh water in the northern Gulf of Mexico. *Journal of Geophysical Research: Oceans*, *108*(C10). https://doi.org/10.1029/2002JC001674

Morey, S. L., Schroeder, W. W., O'Brien, J. J., & Zavala-Hidalgo, J. (2003a). The annual cycle of riverine influence in the eastern Gulf of Mexico basin. *Geophysical Research Letters*, *30*(16). https://doi.org/10.1029/2003GL017348

Murray, S. P. (1972). Observations on wind, tidal, and density-driven currents in the vicinity of the Mississippi River delta. *IN: SHELF SEDIMENT TRANSPORT: PROCESS AND PATTERN*.

Nowlin, W. D., Jochens, A. E., DiMarco, S. F., Reid, R. O., & Howard, M. K. (2005). Low-frequency circulation over the Texas-Louisiana continental shelf. *Circulation in the Gulf of Mexico: Observations and models*, 219-240. https://doi.org/10.1029/161GM17

Ohlmann, J. C., & Niiler, P. P. (2005). Circulation over the continental shelf in the northern Gulf of Mexico. *Progress in oceanography*, *64*(1), 45-81. https://doi.org/10.1016/j.pocean.2005.02.001

Olbers, D. (2005). On the role of eddy mixing on the transport of zonal ocean currents. In *in: Marine Turbulence: Theories, Observations and Models, Ed. H. Baumert, J. Simpson, J. Sündermann, Springer Verlag, Berlin, pp* (pp. 511-529).

Opsahl, S., & Benner, R. (1997). Distribution and cycling of terrigenous dissolved organic matter in the ocean. *Nature*, *386*(6624), 480. https://doi.org/10.1038/386480a0

Ortner, P. B., Lee, T. N., Milne, P. J., Zika, R. G., Clarke, M. E., Podesta, G. P., ... & Johnson, W. R. (1995). Mississippi River flood waters that reached the Gulf Stream. *Journal of Geophysical Research: Oceans*, *100*(C7), 13595-13601. https://doi.org/10.1029/95JC01039

Overland, J. E., & Preisendorfer, R. W. (1982). A significance test for principal components applied to a cyclone climatology. *Monthly Weather Review*, *110*(1), 1-4. https://doi.org/10.1175/1520-0493(1982)110%3C0001:ASTFPC%3E2.0.CO;2

Rabalais, N. N., Turner, R. E., & Scavia, D. (2002). Beyond Science into Policy: Gulf of Mexico Hypoxia and the Mississippi River: Nutrient policy development for the Mississippi River watershed reflects the accumulated scientific evidence that the increase in nitrogen loading is the primary factor in the worsening of hypoxia in the northern Gulf of Mexico. *AIBS Bulletin*, *52*(2), 129-142.

Rabalais, N. N., Turner, R. E., Wiseman, W. J., & Boesch, D. F. (1991). A brief summary of hypoxia on the northern Gulf of Mexico continental shelf: 1985–1988. *Geological*

Society, London, Special Publications, *58*(1), 35-47. https://doi.org/10.1144/GSL.SP.1991.058.01.03

Roemmich, D., & Gilson, J. (2001). Eddy transport of heat and thermocline waters in the NorthPacific: A key to interannual/decadal climate variability? *Journal of Physical Oceanography*, *31*(3), 675-687. *https://doi.org/10.1175/1520-0485(2001)031<0675:ETOHAT>2.0.CO;2*

Ruijter, W. D., Biastoch, A., Drijfhout, S. S., Lutjeharms, J. R. E., Matano, R. P., Pichevin, T., ... & Weijer, W. (1999). Indian-Atlantic interocean exchange: Dynamics, estimation and impact. *Journal of Geophysical Research: Oceans*, *104*(C9), 20885-20910. https://doi.org/10.1029/1998JC900099

Sarkanen, K. V., & Ludwig, C. H. (1971). *Lignins. Occurrence, formation, structure, and reactions*. New York.; Wiley-Interscience.

Schiller, R. V., & Kourafalou, V. H. (2014). Loop Current impact on the transport of Mississippi River waters. *Journal of Coastal Research*, *30*(6), 1287-1306. https://doi.org/10.2112/JCOASTRES-D-13-00025.1

Schiller, R. V., Kourafalou, V. H., Hogan, P., & Walker, N. D. (2011). The dynamics of the Mississippi River plume: Impact of topography, wind and offshore forcing on the fate of plume waters. *Journal of Geophysical Research: Oceans*, *116*(C6). https://doi.org/10.1029/2010JC006883

Schroeder, W. W., Dinnel, S. P., Wiseman Jr, W. J., & Merrell Jr, W. J. (1987). Circulation patterns inferred from the movement of detached buoys in the eastern Gulf of Mexico. *Continental Shelf Research*, *7*(8), 883-894. https://doi.org/10.1016/0278-4343(87)90004-5

Shi, W., & Wang, M. (2009). Satellite observations of flood-driven Mississippi River plume in the spring of 2008. *Geophysical Research Letters*, *36*(7). https://doi.org/10.1029/2009GL037210

Tang, W., Fore, A., Yueh, S., Lee, T., Hayashi, A., Sanchez-Franks, A., ... & Baranowski, D. (2017). Validating SMAP SSS with *in situ* measurements. *Remote Sensing of Environment*, *200*, 326-340. https://doi.org/10.1016/j.rse.2017.08.021

Tréguier, A. M., Deshayes, J., Lique, C., Dussin, R., & Molines, J. M. (2012). Eddy contributions to the meridional transport of salt in the North Atlantic. *Journal of Geophysical Research: Oceans*, *117*(C5). https://doi.org/10.1029/2012JC007927

Walker, N. D. (1996). Satellite assessment of Mississippi River plume variability: causes and predictability. *Remote sensing of environment*, *58*(1), 21-35. https://doi.org/10.1016/0034-4257(95)00259-6

Walker, N. D., and A. B. Hammack (2000), Impacts of winter storms on circulation and sediment transport: Atchafalaya-Vermilion Bay region, Louisiana, U.S.A., J. Coastal Res., 16, 996–1010. http://www.jstor.org/stable/4300118

Walker, N. D., Rouse, L. J., Fargion, G. S., & Biggs, D. C. (1994). The great flood of summer 1993: Mississippi River discharge studied. *Eos, Transactions American Geophysical Union*, *75*(36), 409-415. https://doi.org/10.1029/94EO01045

Walker, N. D., Wiseman Jr, W. J., Rouse Jr, L. J., & Babin, A. (2005). Effects of river discharge, wind stress, and slope eddies on circulation and the satellite-observed structure of the Mississippi River plume. *Journal of Coastal Research*, 1228-1244. https://doi.org/10.2112/04-0347.1

Whitney, M. M., & Garvine, R. W. (2005). Wind influence on a coastal buoyant outflow. *Journal of Geophysical Research: Oceans*, *110*(C3). https://doi.org/10.1029/2003JC002261

Wiseman Jr, W. J., & Dinnel, S. P. (1988). Shelf currents near the mouth of the Mississippi River. *Journal of physical oceanography*, *18*(9), 1287-1291. *https://doi.org/10.1175/1520-0485(1988)018<1287:SCNTMO>2.0.CO;2*

Wunsch, C. (1999). Where do ocean eddy heat fluxes matter? *Journal of Geophysical Research: Oceans*, *104*(C6), 13235-13249. https://doi.org/10.1029/1999JC900062

Yueh, S. H., Tang, W., Fore, A. G., Neumann, G., Hayashi, A., Freedman, A., ... & Lagerloef, G. S. (2013). L-band passive and active microwave geophysical model functions of ocean surface winds and applications to Aquarius retrieval. *IEEE Transactions on Geoscience and Remote Sensing*, *51*(9), 4619-4632. https://doi.org/10.1109/TGRS.2013.2266915

Yueh, S., Tang, W., Fore, A., Hayashi, A., Song, Y. T., & Lagerloef, G. (2014). Aquarius geophysical model function and combined active passive algorithm for ocean surface salinity and wind retrieval. *Journal of Geophysical Research: Oceans*, *119*(8), 5360-5379. https://doi.org/10.1002/2014JC009939**.**

Zhang, W. G., & Gawarkiewicz, G. G. (2015). Dynamics of the direct intrusion of Gulf Stream ring water onto the Mid-Atlantic Bight shelf. *Geophysical Research Letters*, *42*(18), 7687-7695.

APPENDIX A

SUPPORTING FIGURES

CHAPTER 2

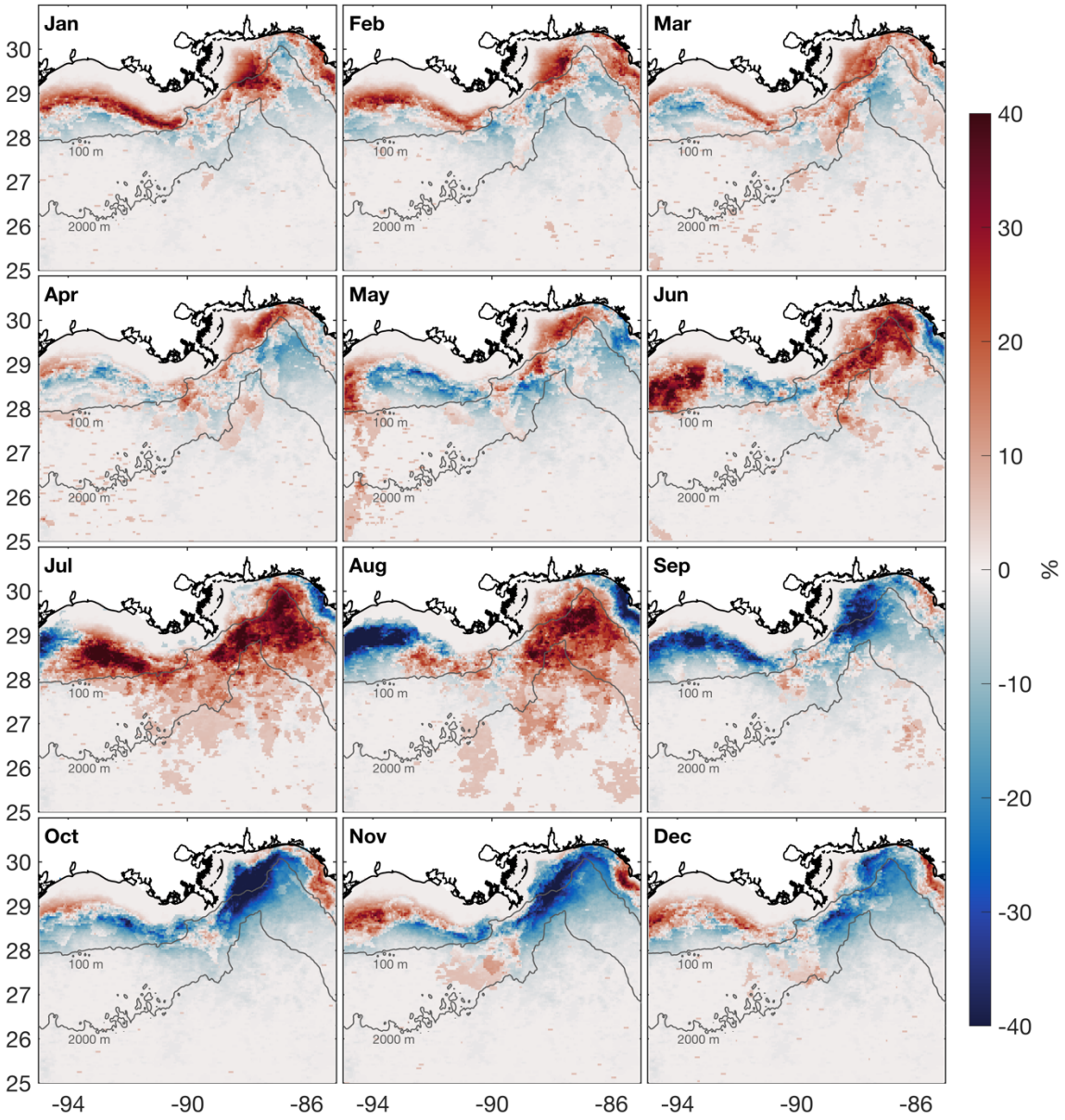

Figure A1. Monthly average anomaly of the frequency of plume occurrence. Anomaly is computed by removing the long-term average.

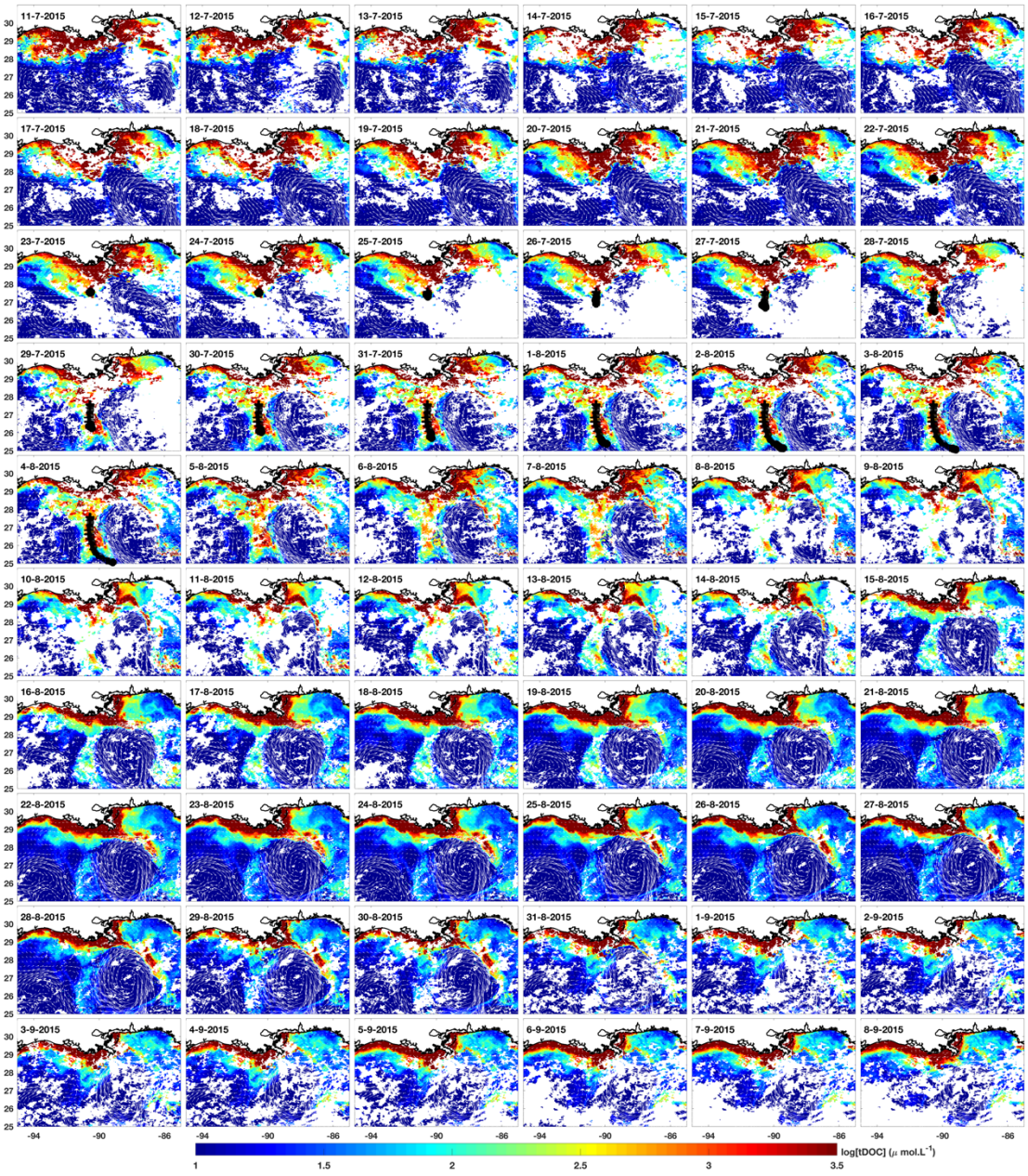

Figure A2. Daily evolution of the MRP during extreme event of offshore transport in 2015 derived from MODIS tDOC. The black line represents the drifter position. Arrows show geostrophic velocity from altimetry.

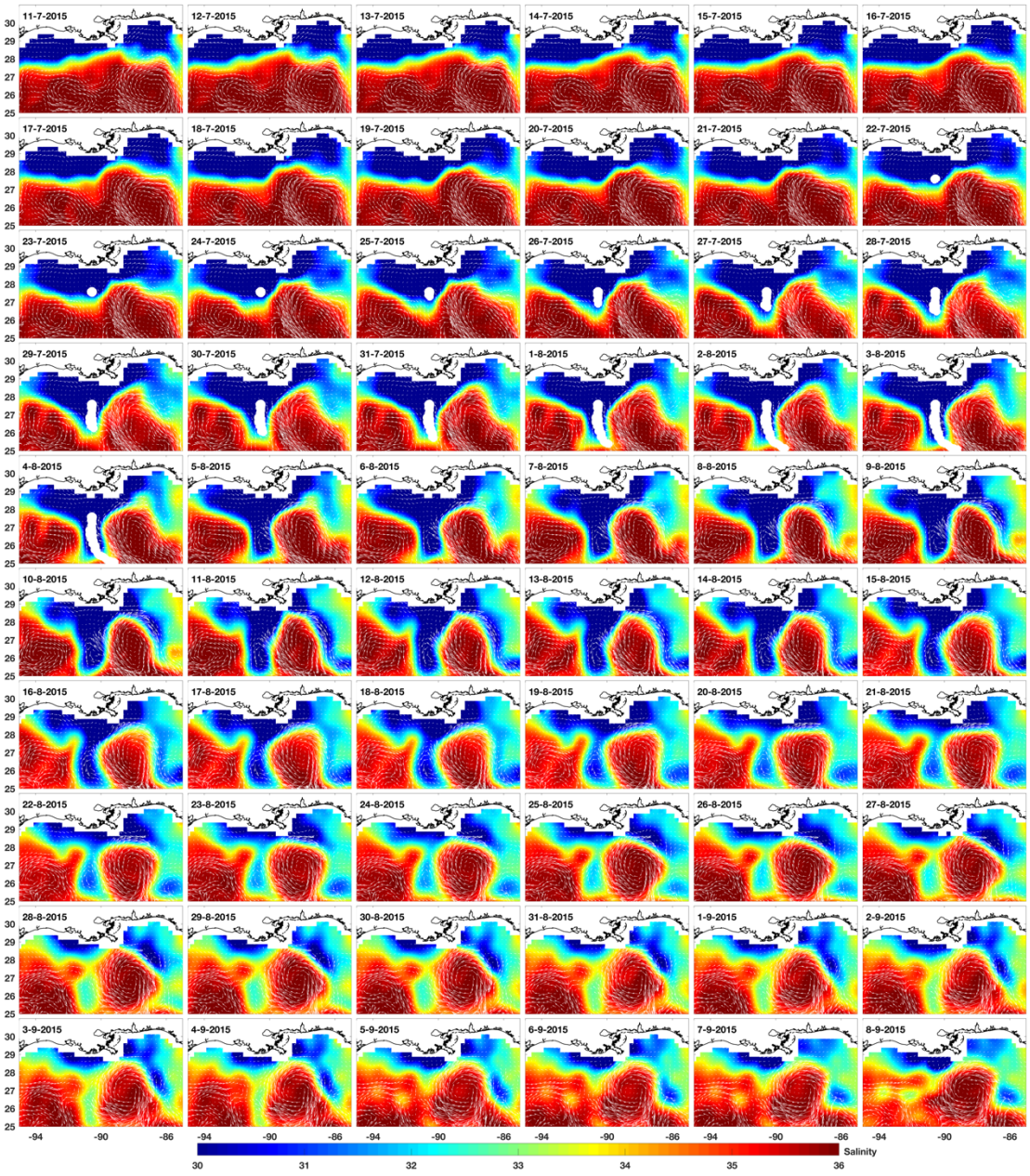

Figure A3. Daily evolution of the MRP during extreme event of offshore transport in 2015 derived from SMAP SSS. The white line represents the drifter position. Arrows show geostrophic velocity from altimetry.

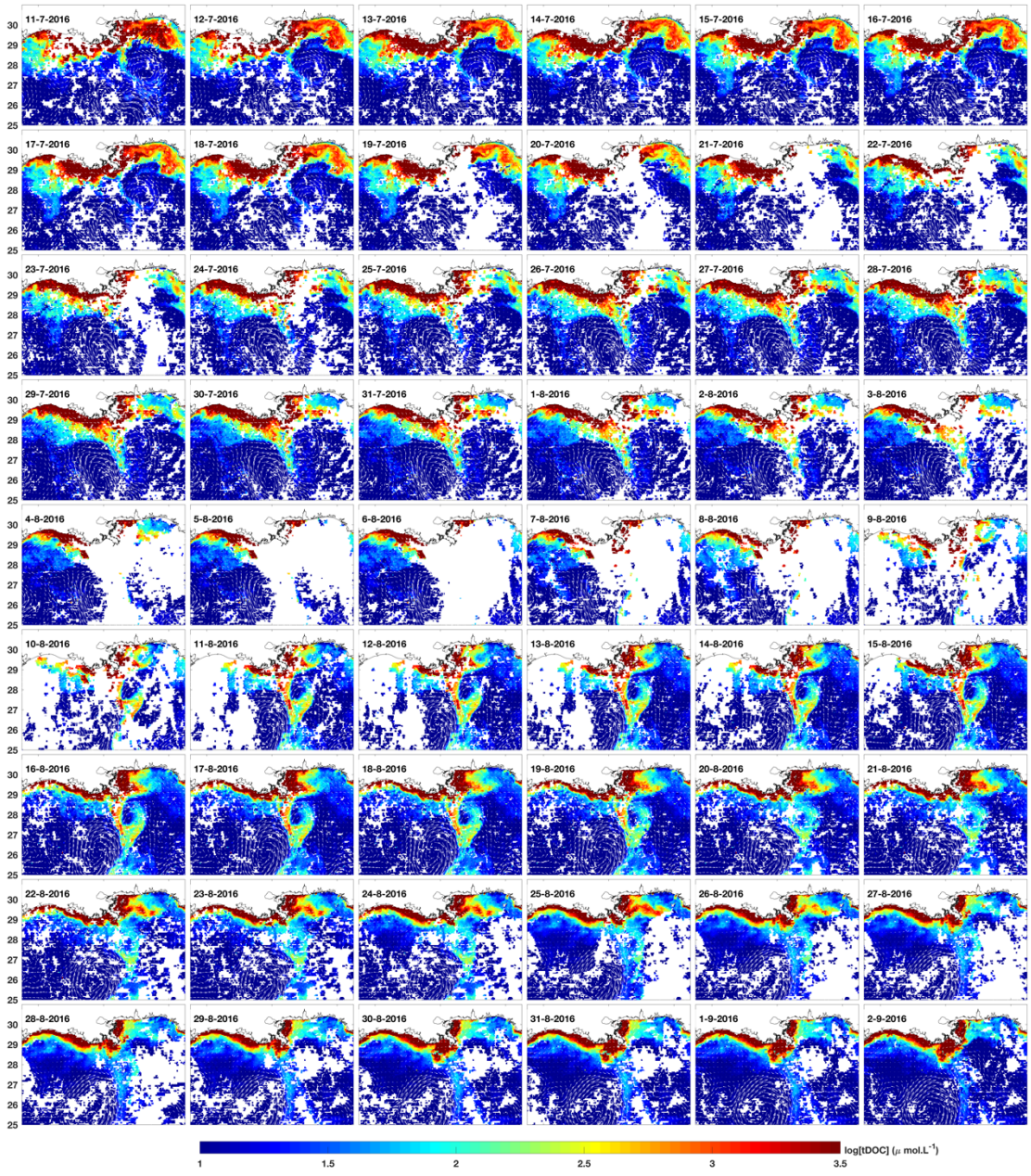

Figure A4. Daily evolution of the MRP during extreme event of offshore transport in 2016 from MODIS tDOC. Arrows show geostrophic velocity from altimetry.

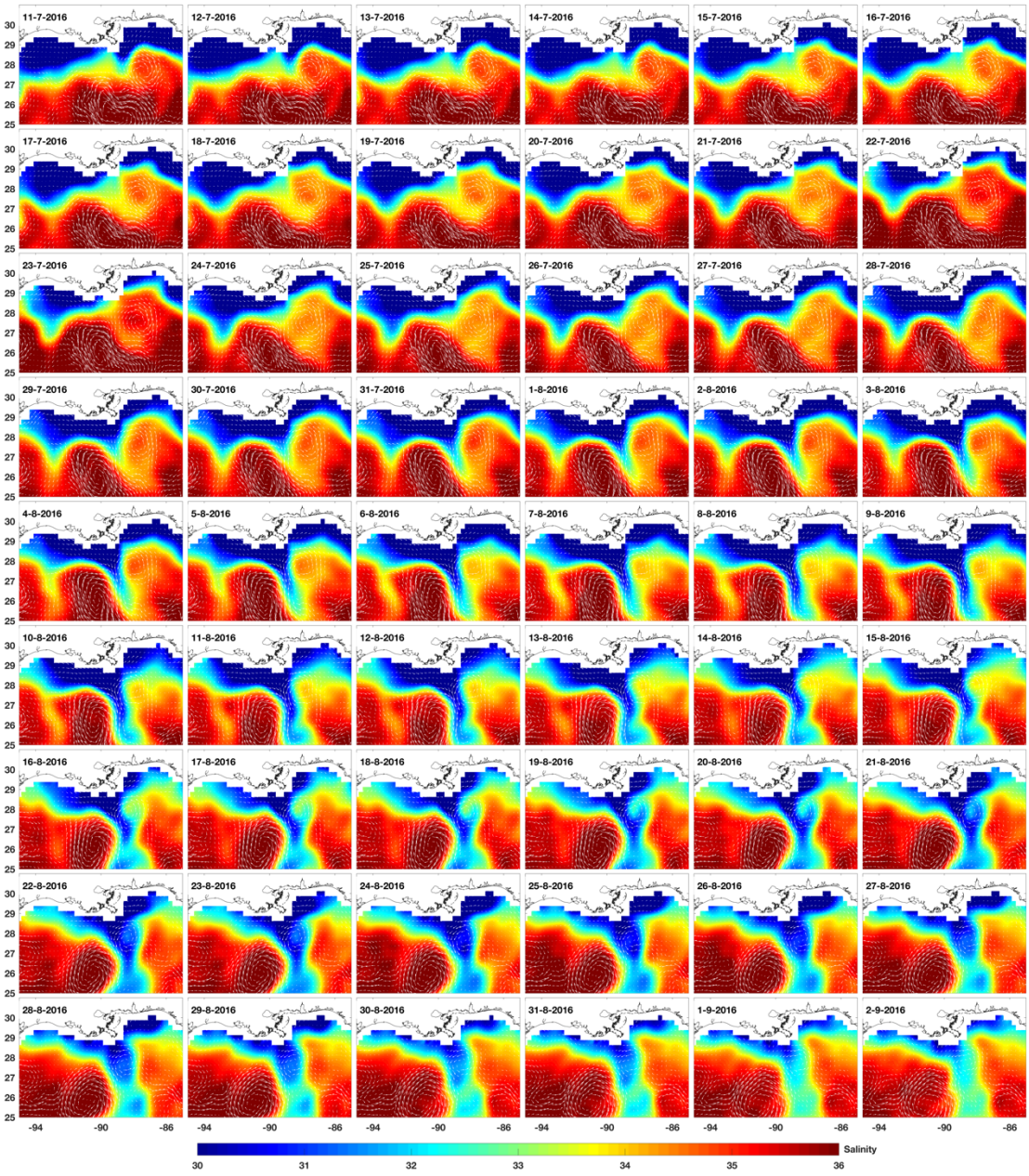

Figure A5. Daily evolution of the MRP during extreme event of offshore transport in 2016 from SMAP SSS. Arrows show geostrophic velocity from altimetry.